OCTOBER 1982
HEWLETT-PACKARD JOURNAL

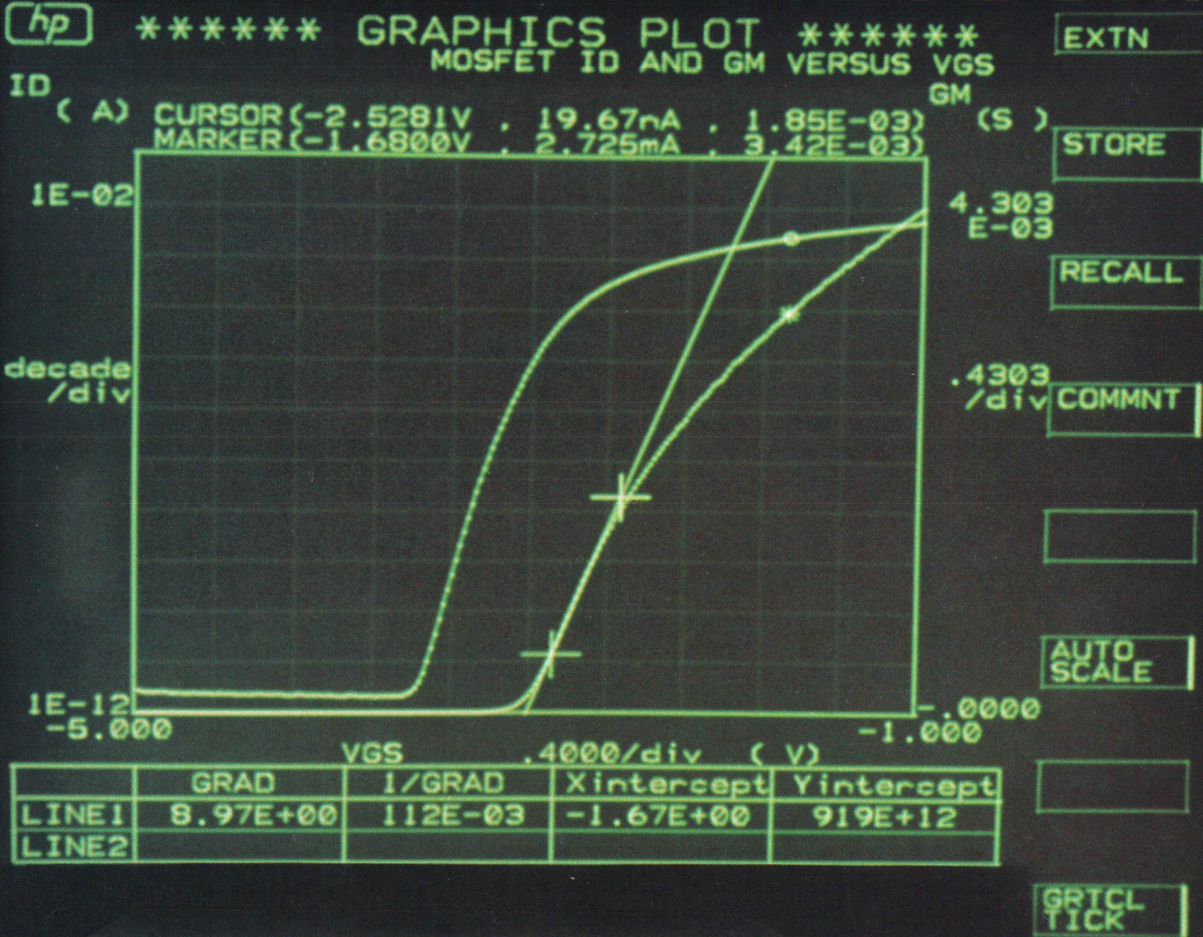

HEWLETT·PACKARD JOURNAL
Technical Information from the Laboratories of Hewlett-Packard Company

OCTOBER 1982 Volume 33 • Number 10

Contents:

3 **Intelligent Instrument Streamlines dc Semiconductor Parameter Measurements,** *by Kohichi Maeda, Jin-ichi Ikemoto, Fumiro Tsuruda, and Teruo Takeda* *Curve-tracer measurements take a quantum leap forward in accuracy and ease of use.*

15 **Programmable Stimulus/Measurement Units Simplify Device Test Setups,** *by Susumu Takagi, Hiroshi Sakayori, and Teruo Takeda* *Each SMU can be electronically set to supply a specified voltage or current and to measure the associated current or voltage.*

21 **HQMOS: A High-Performance NMOS Technology,** *by Horng-Sen Fu, Roger To-Hoi Szeto, Anders T. Dejenfelt, and Devereaux C. Chen* *Smaller NMOS devices operate faster and use less power. Some process innovations are required to make them.*

28 **MOS Device and Process Design Using Computer Simulations,** *by Soo-Young Oh* *The effects of design changes can be accurately predicted by the proper computer model, eliminating the need for actual fabrication.*

In this Issue:

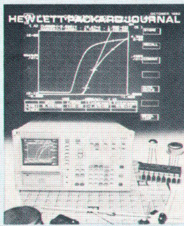

Semiconductor diodes and transistors are the building blocks of the electronic marvels that make our lives easier, more interesting and more productive. The semiconductor is usually silicon, the main component of beach sand, artfully doped with impurities to give it desirable electrical properties. Sometimes diodes and transistors come one to a package as discrete components, and sometimes many are combined in an integrated circuit on a single chip of silicon. In this age of VLSI—very large-scale integration—there may be hundreds of thousands of these devices on a chip, forming a complete microcomputer, memory, or other functional system. Integrated circuits begin their lives as wafers of silicon. Dozens or hundreds of circuits are formed on each wafer in a series of processing steps, and then the wafer is cut apart into individual chips, which are put into packages ready to be assembled into electronic equipment. On our cover this month you can see a wafer and a variety of packaged devices.

The instrument pictured on this month's cover is the 4145A Semiconductor Parameter Analyzer. It's a powerful tool designed to make measurements on transistors and diodes and tell semiconductor manufacturers some of the things they need to know to improve device performance and increase yields (yield is the percentage of chips that operate correctly when they're completed). Parameter measurements are also needed by users of semiconductor devices, who have to know how a device will behave in a circuit, and by people developing computer models of devices for use in computer-aided design systems. The 4145A resembles a venerable instrument called a curve tracer, which has been used for twenty years to measure transistor parameters. However, the resemblance is slight, because the 4145A has a built-in microcomputer and can automatically execute measurement sequences and perform calculations. It can also operate under computer control as part of an automated test system. Engineers who have used a ruler to measure distances on a curve-tracer's screen so they could calculate the slope of a trace are impressed when they find they can position two markers on the 4145A's display and see the slope displayed on the screen. This slope function and the 4145A's ability to display calculated parameters are illustrated in the cover photograph. You can get capability like the 4145A's elsewhere, but only in a sophisticated, expensive system that really represents overkill for many measurement applications. The complete story of the design of the 4145A is on pages 3 to 20.

On page 21 is an article about one of the many processes used to make HP integrated circuits. This process is called HQMOS, for reasons explained in the article, and it was developed by scaling down a standard process, taking advantage of advances in process technology. The scaled-down process produces transistors that operate faster and use less power than those of the standard process.

In the article on page 28 you can find an example of the use of computer models to simulate how process changes may alter device performance. Using these models, process engineers can predict the effects of changes without actually making a wafer.

-R. P. Dolan

Editor, Richard P. Dolan • Associate Editor, Kenneth A. Shaw • Art Director, Photographer, Arvid A. Danielson • Illustrator, Nancy S. Vanderbloom
Administrative Services, Typography, Anne S. LoPresti, Susan E. Wright • European Production Supervisor, Henk Van Lammeren

© Hewlett-Packard Company 1982 Printed in U.S.A.

Intelligent Instrument Streamlines dc Semiconductor Parameter Measurements

Used as a stand-alone instrument or as part of an automated test system, this smart curve tracer makes it easy to measure, analyze, graphically display, and store dc semiconductor parameters.

by Kohichi Maeda, Jin-ichi Ikemoto, Fumiro Tsuruda, and Teruo Takeda

PRECISE DEVICE PARAMETER MEASUREMENTS are essential for computer-aided design and semiconductor research and development, for real-time feedback on wafer evaluations to improve the semiconductor process and increase yields on the production line, and for incoming inspection by end users of semiconductor products. The need for an instrument capable of such measurements that can be used by itself or can be easily incorporated into an automated test system is becoming more and more acute.

The HP 4145A Semiconductor Parameter Analyzer (Fig. 1) was developed to provide an attractive alternative to a curve tracer or an expensive test system, and to satisfy the measurement and evaluation needs of the semiconductor industries. It is a fully automatic, high-performance instrument designed to measure, analyze, and graphically display the dc parameters and characteristics of diodes, transistors, ICs, solar cells and semiconductor materials.

In stand-alone use, the 4145A can rapidly and accurately evaluate a complete range of parameters such as threshold voltage (V_T), transconductance (g_m), common-emitter current gain (h_{FE}), Early voltage (V_A), and many others. See pages 6 and 10 for examples of typical applications. All of the necessary stimulus, measurement, calculation, display, and data storage facilities required are contained in the 4145A. Because the 4145A uses the HP-IB* and HP-GL (Hewlett-Packard Graphics Language), it is easy to interface the 4145A to other measuring instrumentation and controllers for laboratory automation. Publication-quality hard copies of the measurement results displayed on the 4145A's CRT can be obtained simply by connecting an HP-IB-compatible plotter/printer such as the HP 7470A Graphics Plotter and pressing the **PLOT** or **PRINT** keys. The plots for the application examples discussed on pages 6, 7, 10, and 11 were obtained in this manner. No controller is needed. However, by connecting a controller and using simple HP-GL commands, additional information (notes, comments, overlay plots, et cetera) can be displayed on the 4145A's CRT, or the CRT can be used as an independent graphics display.

*Hewlett-Packard Interface Bus, HP's implementation of IEEE Standard 488 (1978)

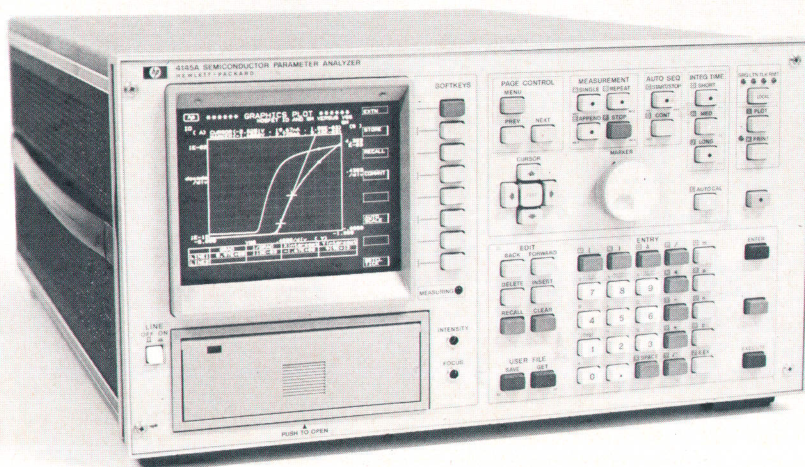

Fig. 1. *The HP 4145A Semiconductor Parameter Analyzer is the first stand-alone instrument capable of fully automatic measurements of dc semiconductor parameters. Using the Hewlett-Packard Interface Bus (IEEE 488), it can also form part of a larger computer-controlled test system for parameter evaluation, comparison, and storage.*

Features

Some of the features of the 4145A are:

- Four stimulus/measurement units (SMUs) that can be programmed to perform in one of three different modes:
  1. Voltage source and current monitor (V mode)
  2. Current source and voltage monitor (I mode)
  3. Common connection (COM mode).
- Two voltage sources (VS) that can be linearly or logarithmically swept over their programmed output range.
- Two voltage monitors (VM).
- High-resolution digital CRT display module for displaying graphic and alphanumeric information in any of five different display modes: graphic display, matrix display, schmoo* plot, list display, and time domain. The display can also be programmed by an external controller using HP-GL commands.
- Internal flexible disc drive for storing measurement setups, autosequence programs, and data.
- Built-in HP-IB interface for easy connection of the 4145A to other HP-IB-compatible instruments and controllers to form automated test systems.
- Eight built-in functions to simplify control and manipulation of the displayed data.
- Two user functions that allow front-panel programming of two different arithmetic operations for calculating parameters from measured values. The results can be displayed in real time versus the measured values.
- Versatile front-panel keyboard for measurement setup and manipulation of displayed data. Eight softkeys along the right side of the display make it easy for an operator to select the desired test conditions and display format.

*A three-dimensional plot in which Z-axis values are indicated by different symbols on an X-Y plot.

Hardware Architecture

A block diagram of the 4145A's hardware system is shown in Fig. 2. The digital system is functionally divided into six blocks: the main processing unit, graphic display unit, mass storage unit, front-panel unit, and HP-IB interface contained in the digital section, and the SMU controller located in the measurement section and coupled to the rest of the digital system through an optoisolator.

The main processing unit uses a 68B00 microprocessor and contains 16K bytes of ROM, 32K bytes of dynamic RAM, a 10-ms interval timer, and the SMU controller interface.

The graphics display unit contains an HP 1345A Digital Display Module[1] and a two-port read/write 4K×16-bit vector memory to store picture data. The 1345A picture data is refreshed automatically by scanning the vector memory at a rate of approximately 50 Hz.

A keyboard, rotary pulse generator, and various indicators make up the front-panel unit. The keyboard consists of a number of keys arranged in convenient groupings for page control, measurement control, autosequence control, integration-time selection, editing, alphanumeric and arithmetic operation entry, autocalibration, print/plot control, softkeys, file storage and retrieval, and cursor positioning. The rotary pulse generator outputs 120 pulses per revolution and controls the display marker. The indicators show the current HP-IB status and selected operations.

The mass storage unit contains a flexible disc controller and drive. The drive handles 5.25-in, single-sided, single-density, flexible discs having a storage capacity of 92 kilobytes on 40 tracks with 9 sectors per track, 256 bytes per sector.

The SMU controller is the measurement controller in the 4145A. It uses a 6802 microprocessor and contains 12K bytes of ROM, 1K byte of static RAM, two analog interfaces,

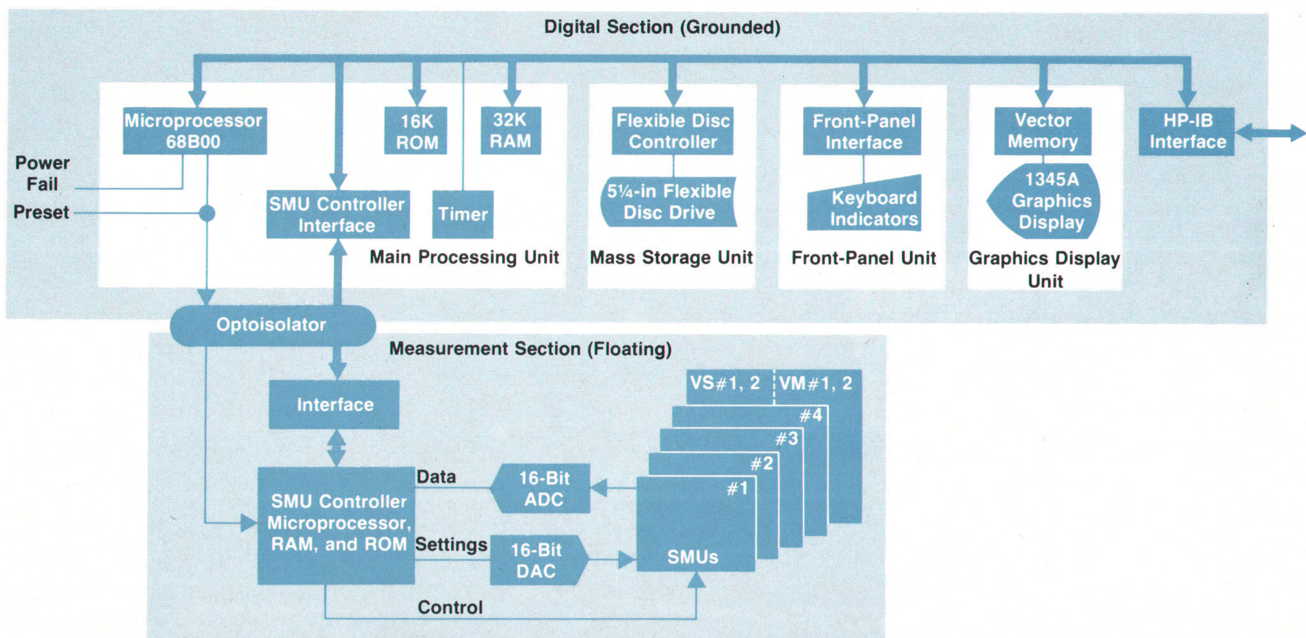

Fig. 2. *Block diagram of the 4145A's hardware system consisting of a grounded digital section and a floating measurement section. Communication between the two sections is through an optoisolator.*

and an asynchronous communication interface capable of a data transmission rate of 250,000 bits/s. The two analog interfaces are used to communicate with the four SMUs, two VSs, and two VMs via analog-to-digital and digital-to-analog converters as shown in Fig. 2. The asynchronous interface is ground-isolated and connected to the system microprocessor in the main processing unit by optoisolators. This arrangement allows floating-ground measurements.

The SMU controller has intelligent functions that enable the system processor to give commands or get data with ease. For example, it has sweep control capability. Once the SMU controller has been given sweep parameters (linear/log, start value, step size, number of steps), it sets up the source output values, gives hold or delay time, measures monitored values, and reports measurement data automatically at every step.

A second feature is the line-frequency-synchronized sampling and averaging technique to reduce ac line noise. When **INTEG TIME** is set to **SHORT**, the measured data is stored directly without integration. However, when **INTEG TIME** is set to **MED**, 16 samples are taken during one ac line frequency cycle and averaged for each measurement value. The **LONG** setting averages 256 samples taken during 16 ac line cycles. The sample timing is controlled by a timer that counts the main processing unit clock pulses.

Another feature is SMU dc offset correction. The SMU controller calibrates all dc offsets in the SMUs and cancels these parameters on every setting and measurement. Consequently there are no adjustable components on the SMU assemblies. This improves the long-term stability of the dc offset error specification.

The SMU controller also has a self-test function. Self-test consists of two parts. One is the test of the SMU controller itself and the analog-to-digital and digital-to-analog converters interfacing the SMU controller to the SMUs, and the other is the SMU test. If an error occurs in the former test, the SMU controller shuts down operation because this kind of error is a fatal error. The system processor detects this state and displays A01 on the CRT, indicating that the SMU controller is down. The light-emitting diodes (LEDs) on the SMU controller board show the error number, which indicates the error block. In the SMU test, detected errors are not fatal to system operation. The SMU controller simply reports the results of the test and system operation continues. At this time, the CRT display shows the error number, if any, for each SMU.

The measurement section is divided into seven blocks (excluding the SMU controller): an analog-to-digital converter (ADC), a digital-to-analog converter (DAC), four SMUs, two VSs and two VMs. The 16-bit ADC is combined with a 10-channel multiplexer. The multiplexer selects one channel from the 10 channels connected to the four SMU voltage monitor outputs, the four SMU current monitor outputs and the two VM outputs. Digital data from the ADC is sent to the digital section to be processed and displayed.

To obtain both high resolution and high speed from a simple hardware configuration, the ADC in the 4145A uses a special input range expansion technique. As shown in the block diagram in Fig. 3a, the ADC is of the successive approximation type. It uses two DACs. One is a 14-bit

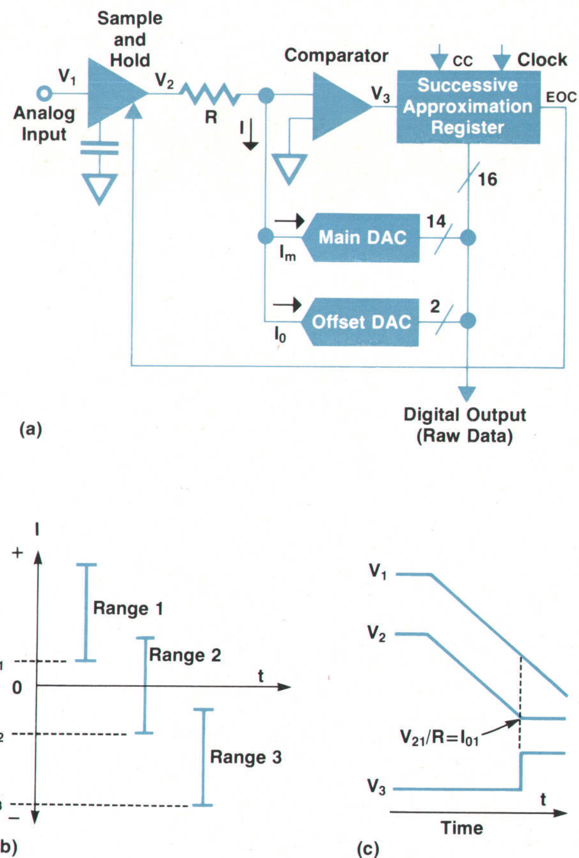

Fig. 3. *(a) Block diagram of the ADC used in the measurement section of the 4145A. The conversion is done by successive approximation, using DACs to supply the error signal to the comparator. (b) By setting I_{01}, I_{02}, and I_{03} in turn, the error signals to correct the offset of the ADC can be derived. (c) Relationship of the voltages V_1, V_2, and V_3 shown in (a) for the first sample-and-hold period.*

monotonic main DAC and the other is an offset DAC for input range expansion. The offset DAC outputs three offset current values that provide three expanded ranges. Within each range, the main DAC has 14-bit resolution. The raw digital data is output as 2 bits of offset range data plus 14 bits of main data. To convert this intermittent binary data into consecutive data over the full input range, the microprocessor has to know the offset value for each range.

To measure these offset values, a self-calibration is performed. First, the main DAC's output current I_m is set to zero and the offset DAC's output current I_0 is set to I_{01} (see Fig. 3b). At this time, the sample-and-hold circuit is set to the sample mode and a ramp voltage is applied to its input. The comparator output goes high at the balancing point (i.e., $V_{21}/R = I_{01}$). At this moment, the sample-and-hold circuit is set to the hold mode. Then the output current of the offset DAC is changed to I_{02}, and a successive approximation conversion is performed using the main DAC. The result of this conversion gives the relative offset value between I_{01} and I_{02}. Similarly, the second step of the calibration process determines the difference between the I_{02} and I_{03} values of the offset DAC. In addition, the absolute offset value can be measured by the normal analog-to-digital con-

Typical Applications of the 4145A Semiconductor Parameter Analyzer

Four examples of common semiconductor device measurements done by the 4145A are shown in Fig. 1 through Fig. 4. The first two examples evaluate characteristics of a bipolar npn transistor and the remaining two examples evaluate an MOS device. Part (a) of each figure is a hard copy of the 4145A's graphic display and part (b) shows the 4145A test connections and SMU mode settings to the device under test.

Static Collector Characteristics

The static collector characteristics of a bipolar transistor are shown in Fig. 1. They were obtained by linearly sweeping the collector voltage V_{CE} from 0 to 10V at five different values of base current I_B and measuring the resulting collector current I_C. SMU-1 is programmed for operation as a common source (COM mode), to which all other sources in the measurement are referenced. SMU-2 is used as a variable current source (I mode) to provide the requisite base current. SMU-3 acts as a variable voltage source (V mode) and current meter to provide collector voltage and measure the collector current. SMU-3 is the primary sweep source VAR1 and SMU-2 is the secondary, or dependent, sweep source VAR2. The VAR2 source is incremented only after each VAR1 source sweep. By using the 4145A's built-in line function to draw a straight line between points A and B, the transistor's collector output resistance and Early voltage can be read directly from the 1/GRAD and X-INTERCEPT values, respectively. In this example, the output resistance is 9.37 kΩ and the Early voltage is −77.7V.

h_{FE}-I_C Characteristics

By using one of the two internal user functions, a bipolar transistor's h_{FE}-I_C curve can be obtained (Fig. 2). h_{FE} is defined as I_C/I_B. The h_{FE} decay constant can be read directly from the 4145A's CRT display by using the line function to draw a line tangent to the linear portion of the curve as shown in Fig. 2a.

MOS Threshold Characteristics

The five curves shown in Fig. 3 represent an MOS device's characteristics at five different substrate voltages V_{SB}. The threshold voltage V_T of an enhancement-type MOSFET is defined as the gate voltage required to cause a predetermined value of drain current (in this example, 10 μA). V_T can be obtained by

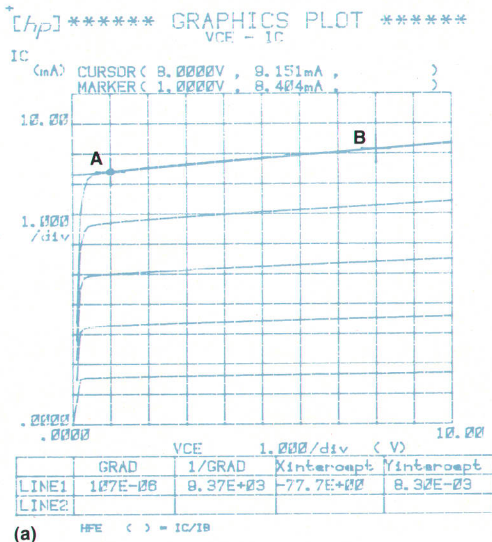

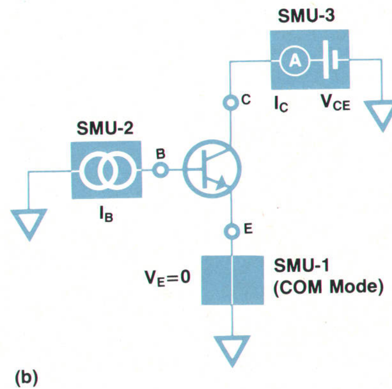

Fig. 1. *(a) Linear graphics display for static collector characteristics measurement of an npn bipolar transistor. Cursor is at point B, marker at point A. (b) Source setup values and test configuration for (a).*

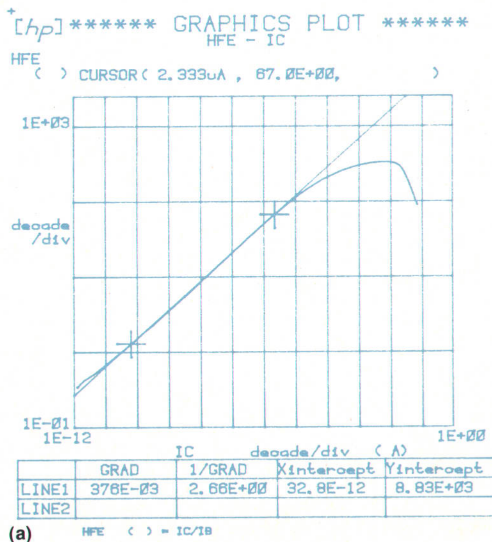

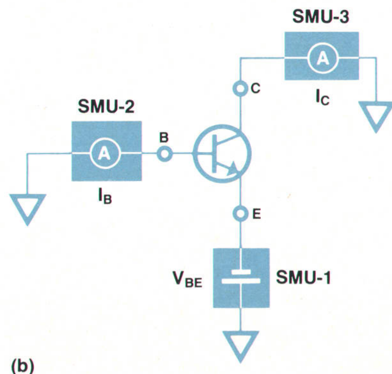

Fig. 2. *(a) h_{FE} versus I_C display for a npn bipolar transistor. Both axes are logarithmic. (b) Source setup values and test configuration for (a).*

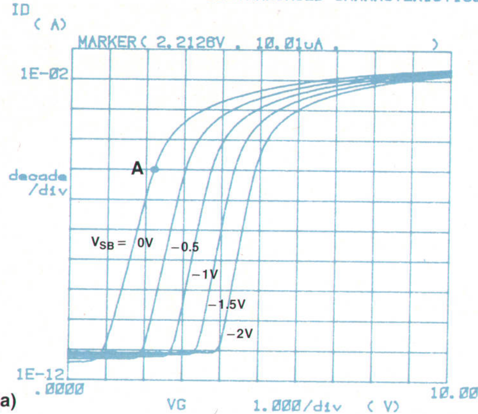

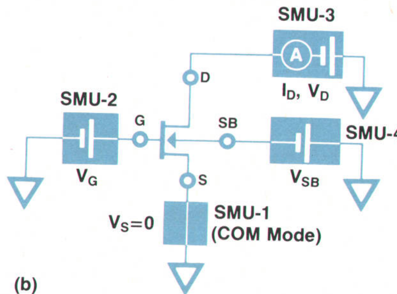

Fig. 3. *(a) Log-linear display of MOSFET threshold characteristics for five different substrate voltages. (b) Source setup values and test configuration for (a).*

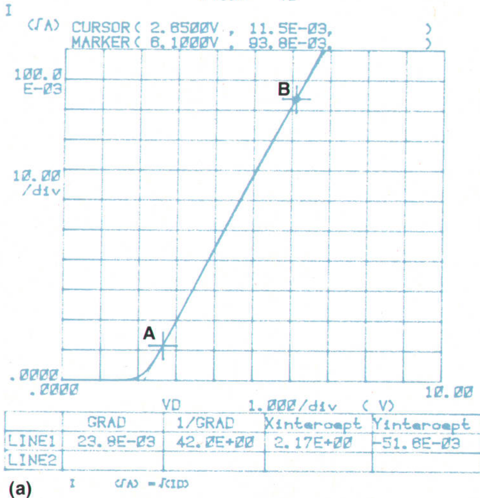

	GRAD	1/GRAD	Xintercept	Yintercept
LINE1	23.8E-03	42.0E+00	2.17E+00	-51.6E-03
LINE2				

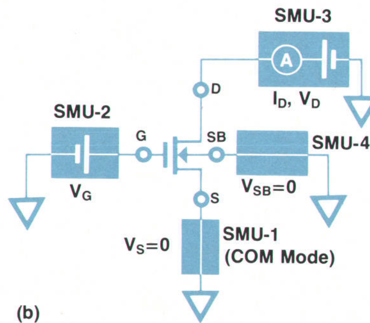

Fig. 4. *(a) Linear display for determining threshold voltage of an MOS device (see text). Cursor is at point A, marker at point B. (b) Source setup values and test configuration for (a).*

moving the display marker along the curve until $I_D = 10\ \mu A$ (point A), and then reading the value V_G at that point as displayed numerically above the graph. In Fig. 3, V_{T0} ($V_{SB} = 0$) is 2.213V.

Threshold Voltage V_T

Another method of measuring V_T is to bias the MOSFET such that the gate and drain are always at the same potential and measure the characteristics in the saturation region. Drain current in the saturation region is calculated as

$$I_D = \beta(V_{GS} - V_T)^2$$

where β is the gain factor of the device. By taking the square root of this equation, we find that the relationship between $\sqrt{I_D}$ and V_{GS} is linear, the slope of the line is $\sqrt{\beta}$, and the point at which the line crosses the X-axis is V_T. Thus

$$\sqrt{I_D} = \sqrt{\beta}\,(V_{GS} - V_T)$$

The 4145A's user function can be set up to perform this calculation during the measurement. From Fig. 4, X-INTERCEPT shows a V_T of 2.17V. The square of the line GRAD is $\beta = 566 \times 10^{-6}$.

version of zero input, which is shown in Fig. 3b as I_{02}. From these values, the microprocessor is able to determine the absolute offset value of each range, and to get true data by simple addition or subtraction. Thus, this ADC can measure approximately ±11 volts full scale with 0.5-mV resolution and 200-μs conversion speed.

The 16-bit DAC is used by the SMU controller to output control settings. It has a 10-channel distributor that allocates outputs from the DAC to each SMU and VS input.

The four stimulus measurement units are the heart of the 4145A. Each SMU can be programmed to function as a voltage source and current monitor (V mode) or a current source and voltage monitor (I mode). In the V mode, an SMU can supply from ±1 mV to ±100V over three output ranges as given in Table I. In the I mode, currents as low as 1 pA and as high as 100 mA can be forced as listed in Table II. If higher currents or voltages are required, an SMU can be used to program an external power supply (see box on page 10). One advantage of the SMU concept is that a four-terminal device can be completely characterized by the 4145A without changing connections. For example, a bipolar transistor can be characterized in common-base, common-collector, and common-emitter configurations without any connection changes. See the article on page 15

Table I
SMU Output Capability: V Mode

Voltage Range	Resolution	Accuracy	Maximum Current I_o
±20V	1 mV	±(0.1% of reading	100 mA
±40V	2 mV	+0.05% of range	50 mA
±100V	5 mV	$+0.4\Omega\times I_o$)	20 mA

I_o=output current at set voltage.

Table II
SMU Output Capability: I Mode

Current Range	Resolution	Accuracy	Maximum Voltage V_o
±100 mA	100 μA	±[0.3% of reading +(0.1+0.002V_o)% of range]	20V(I≤100 mA) 40V(I≤40 mA)
±10 mA ±1000 μA ±100 μA ±10 μA	10 μA 1 μA 100 nA 10 nA		100V (I≤20 mA)
±1000 nA ±100 nA	1 nA 100 pA	±[0.5% of reading +(0.1+0.002V_o)% of range]	
±10 nA ±1000 pA	10 pA 1 pA	±[5 pA+1% of reading +(0.1+0.002V_o)% of range]	

V_o=output voltage at set current.

for a discussion of the design of the SMUs.

As mentioned earlier, the output from each SMU is determined by two input control voltages from the 16-bit DAC, one for output voltage and one for output current. Other information, such as voltage or current ranging, is given directly by the SMU controller. Each SMU outputs two monitor voltages to the 16-bit ADC that correspond to SMU output voltage and output current.

The two additional voltage sources (VS) and two voltage monitors (VM) are built in for measurements that require more sources and/or monitors than provided by the four SMUs. Each VS is a programmable voltage source whose ±1 mV to ±20V output is determined, like the SMUs', by the output from the 16-bit DAC. Each VM is similar to a buffer amplifier whose monitor output is sent to the ADC via the multiplexer. Each VM can measure voltages from ±100 μV to ±2V, or from ±1 mV to ±20V, depending on its range setting.

Software System

The 4145A's software system (Fig. 4) is based on a real-time monitor whose functions are as follows:

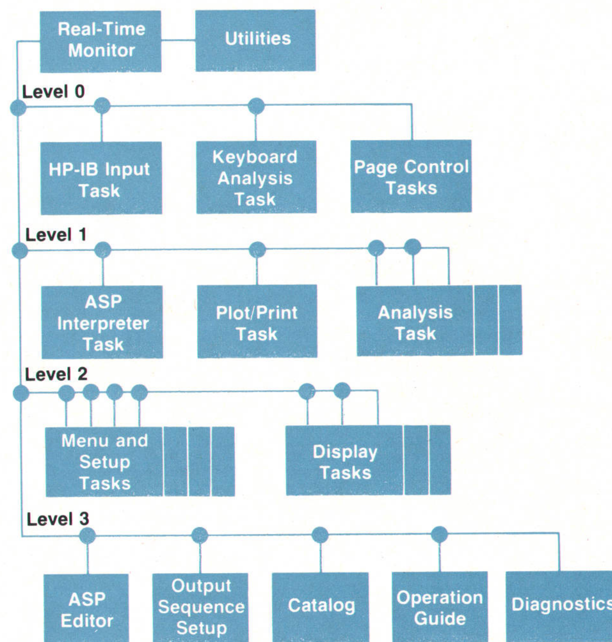

Fig. 4. *The software architecture of the 4145A is based on a real-time monitor to control the utilities and four priority levels of tasks (ASP=Autosequence program).*

- Task management (multitasking). A task is the primary structure of an execution environment under the real-time monitor. The monitor supports multitasking operations with four priority levels. Eight tasks are available for each level. Task management services include start, end, and abort.
- Task synchronization. Tasks can communicate information to another task via an event control block, which is managed by the real-time monitor and not visible to a task programmer. The receiving task calls the WAIT macrocommand with the event control block number. The sending task calls the POST macro with the event control block number and a post code.
- Program management. Certain tasks are resident on the flexible disc. If one of these tasks is required but is not already in the overlay area (see Fig. 5), the program manager loads the appropriate file containing the task and starts it.
- Timer services. The real-time monitor can periodically initiate execution of a specified task. This is a very important function for measurement instrumentation. The monitor can also suspend task execution for a specified interval and initiate execution of a specified task after a specified interval.
- Interrupt handling. The interrupt handler monitors and processes interrupts from the powerfail detector, timer, HP-IB, and asynchronous communication interface. Up to eight interrupt processing routines can be supported.
- I/O control. The I/O control subsystem provides the basic drivers and various utilities to control the instrument hardware, graphics display, mass storage, front panel, and asynchronous communication interface.

The 4145A has a memory-mapped I/O system and 16K

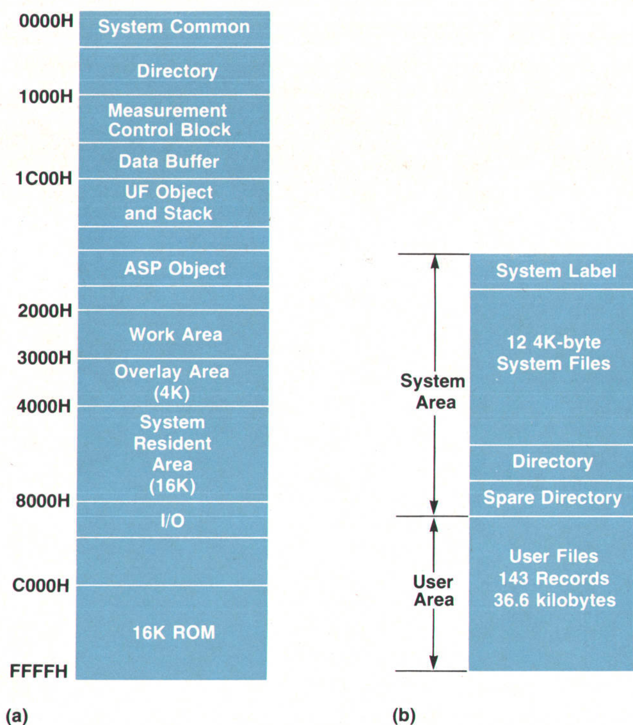

Fig. 5. *(a) Memory map for main processing unit. (b) Disc memory structure for the single-sided, single-density, 5.25-in flexible discs used by the 4145A's internal disc drive.*

bytes (4K×4) of ROM. The ROM area contains the real-time monitor, I/O control, power-on self-test programs, and some frequently used utilities.

The 4145A's memory map is shown in Fig. 5a. The directory is a copy of the directory stored on the disc. If the disc is changed, the directory is automatically revised at the next file access. The measurement control block contains the control information for a measurement. Data in this block is changed by changing the information on the CHANNEL DEFINITION, SOURCE SET UP, MEAS & DISP MODE SET UP, OUTPUT SEQUENCE SET UP and DISPLAY menu pages. This area (768 bytes) can be stored on the disc by the command SAVE P Filename. Measurement data is stored in the data buffer (2304 bytes). The measurement control block and the data buffer can be stored on the disc by the command SAVE D Filename. The UF object and stack area (256 bytes) is used as an intermediate code area for user functions and as a stack area for RPN (Reverse Polish Notation) operation. The intermediate code of the autosequence program is resident in the ASP object area (256 bytes). This area can be stored on the disc by the command SAVE S Filename. Nonresident tasks and data are loaded into the overlay area by the real-time monitor before execution. Resident tasks, common data and utilities are loaded into the system resident area at instrument power-on.

The 4145A uses an internal single-sided, single-density flexible disc drive to store system programs, measurement data and user programs. The disc space is divided into a system area and a user area (see Fig. 5b). The system area consists of a system label, 12 system files and a directory. Files in the user area are organized by an indexed access method. The size of each system file is 4K bytes, including tasks, utilities and data. The directory is provided for user area management with a spare directory for backup. The size of the directory is 2K bytes.

The user area has room for 143 records (256 bytes/record). The first 12 records are reserved for system default programs. The 4145A has three types of user files: program files (3 records), data files (12 records) and sequence files (1 record). Up to 43 program files can be stored on each disc. Each file has a unique name (6 characters maximum). The following commands and the catalog function (see Fig. 6) are provided for management of these user files.

SAVE	P/D/S	Filename	for storing user files
GET	P/D/S	Filename	for retrieving user files
PURGE	P/D/S	Filename	for purging user files
REPACK			for repacking the user area

P indicates a program file, D indicates a data file, and S indicates a sequence file.

Instrument Operation

There are two important points to consider when designing a keyboard-operated instrument. One is simplicity and ease of use, making the measurement complexity transparent to the inexperienced or casual user. The other is versatility for more experienced users and sophisticated measurements.

The operating system of the 4145A is designed to perform a wide range of operations with menu-driven, softkey-oriented control. The measurement procedures are divided functionally into four parts that are each displayed in a menu page format: CHANNEL DEFINITION, SOURCE SET UP, MEAS & DISP MODE SET UP, and DISPLAY (see Fig. 7). These pages can be accessed sequentially by pressing the **PREV** or **NEXT** keys, and directly from the menu page by pressing the appropriate softkey. The user sets up, or programs, the measurement by filling in blanks on each menu page. The

[hp] *** USER FILE CATALOG ***

available records 25

name	typ	comments	adrs	rsv	usd
GENL	sys	system	217	3	3
BVCEIC	sys	system	220	3	3
FVDSID	sys	system	223	3	3
DIVFIF	sys	system	226	3	3
BIP1	Seq	DEMO 1	229	1	1
BIP2	Seq	DEMO 2	230	1	1
BIPTD	Seq	FOR T/D	231	1	1
BIP	Seq	FOR A/N	232	1	1
NPN1	Pro	*APP 1	233	3	3
ICBVBE	Pro	*APP 2	236	3	3
EMTR	Pro	*APP 3	239	3	3
COLR	Pro	*APP 4	242	3	3

Fig. 6. *Typical directory listing of files stored on a flexible disc. Each disc contains the operating system for the 4145A in addition to saved user programs and stored data.*

Extending the 4145A's Output Range for Power Transistor Measurements

Each of the 4145A's stimulus/measurement units (SMUs) is capable of supplying up to 100 mA or ±100V, with a maximum power output of 2W. This is more than sufficient for stimulating and measuring low-power semiconductor devices, which account for perhaps 90% of semiconductor products. To cover the remaining 10%, which consists mainly of power transistors and diodes, the 4145A's output capabilities must be increased. This can be accomplished simply and economically.

The method requires no controller or interface. The only equipment needed is the 4145A, its furnished accessories, and a suitable power supply that can be controlled by an analog voltage and has a current-monitoring terminal, such as HP's 6024A Autoranging DC Power Supply. Fig. 1 shows the setup.

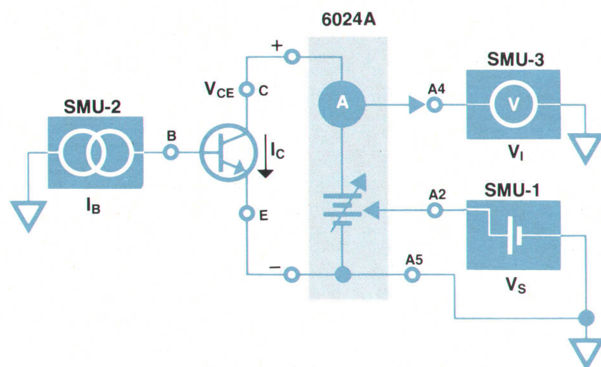

Fig. 1. *Test configuration using HP 6024A Autoranging DC Power Supply controlled by the 4145A's SMUs, effectively boosting the output current and voltage range of the 4145A for power transistor measurements.*

Three of the 4145A's SMUs are used. SMU-2, programmed to function as a variable current source, drives the base of the transistor being measured. SMU-1, programmed to function as a variable voltage source, is connected to the 6024A's remote control (analog programming) terminal A2 to provide the voltage necessary to control the 6024A's output voltage. Output voltage from the 6024A is directly proportional to the voltage (V_S) supplied by SMU-1 and can be calculated as

$$V_{6024A}=12\times V_S=V_{CE} \quad (1)$$

Thus, by sweeping the SMU-1 voltage from 0V to +5V, the 6024A's output can be swept from 0V to 60V. SMU-3, programmed to function as a voltage monitor, is connected to the 6024A's current-monitor terminal A4. The 6024A's output current is directly proportional to the voltage (V_I) measured at this terminal by SMU-3 and can be calculated as

$$I_{6024A}=2\times V_I=I_C \quad (2)$$

The 6024A's outputs are connected to the collector and emitter of the transistor as shown in Fig. 1.

By using the two internal user functions of the 4145A to calculate the output voltage and current by equations (1) and (2), the actual values applied to the transistor tested can be displayed directly. The results of an actual measurement using this setup are shown in Fig. 2. Maximum current through the transistor is approximately 1A and power is close to 1W. Higher current and power can be obtained by increasing the base drive current I_B and/or the control voltage V_S. Fig. 3 shows the results of a high-power—over 40W—measurement.

There are several points concerning safety and accuracy that must be kept in mind when using this method.

1. Depending on the forward transfer gain h_{FE} of the transistor under test, current levels up to 10A are possible with this setup. Be sure to close the lid of the 16058A Test Fixture before starting the measurement and do not touch the connection plate.
2. Because of the high current flow, there will be an unavoidable voltage drop across the residual resistance of the test leads and cables. This voltage drop represents a measurement error. The actual collector-emitter voltage V_{CE} is calculated as

$$V_{CE}=V_{OUT}-I_{OUT}\times R$$

where V_{OUT} is the 6024A's output voltage, I_{OUT} is the output current, and R is the total residual resistance of the leads, cables, and test fixture. By using the 4145A's remaining SMU and one of its voltage monitors for voltage sensing at the collector and emitter, this error can be reduced to almost zero.

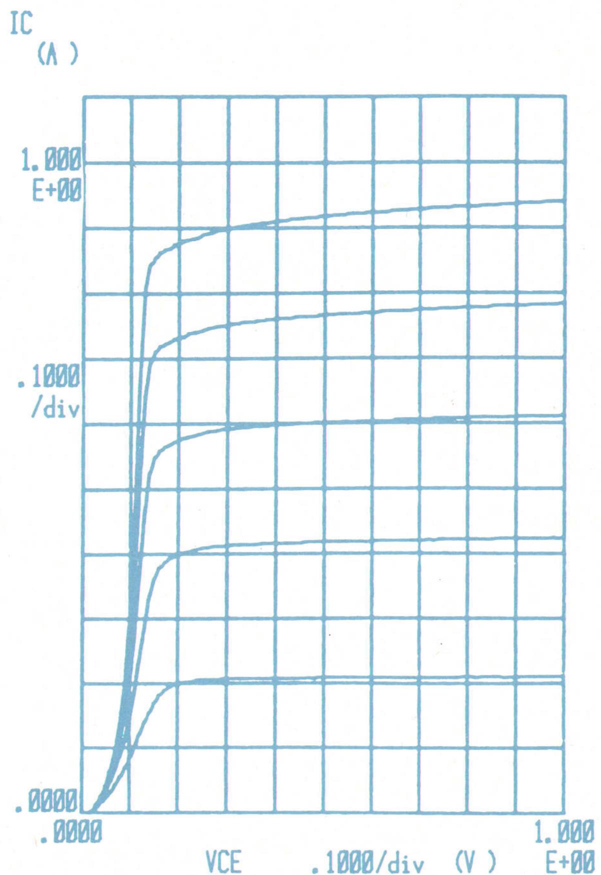

Fig. 2. *Typical graphics display of results obtained with test setup shown in Fig. 1. Low-voltage V_{CE} characteristics at collector currents up to 10A are easily shown.*

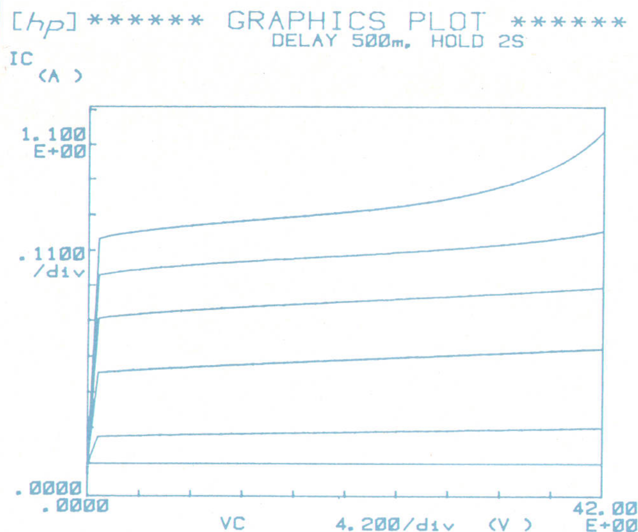

Fig. 3. *Result of a high-power measurement using the setup in Fig. 1. The control voltage V_S is swept from 0V to 3.5V in 0.07V steps and I_B is swept from 1 mA to 9 mA in 2-mA steps.*

To do this, however, the test setup and the user function calculating V_{CE} must be changed slightly (Fig. 4). SMU-4 is connected to the collector of the transistor and set up in the I mode as a constant current source at 0.0A with a compliance of 100.00V. This allows it to behave as a voltage monitor. One of the 4145A's two voltage monitors is connected

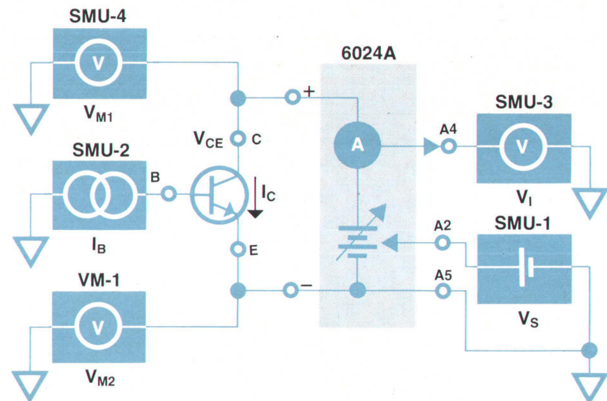

Fig. 4. *Revised Fig. 1 setup to correct for voltage-drop error introduced by high current flowing through the test leads and connectors. By measuring the voltage across the transistor directly, using SMU-4 and VM-1, this error can be eliminated.*

to the emitter of the transistor and the user function for V_{CE} is changed from $V_{CE}=12\times V_S$ to $V_{CE}=V_{M1}-V_{M2}$.

3. Wait until the transistor has sufficiently cooled before making additional measurements. Heat generated by high current flow drastically affects the transistor's parameters, especially h_{FE} and I_{CBO}. Thus, if the measurement is repeated before the transistor has cooled, measurement results will differ significantly.
4. Set the 4145A to **MED** or **LONG** integration time to reduce the effects of ac line frequency noise on the measurement.

-Michitaka Obara

field pointer (▶) and system messages displayed on the CRT guide the operator through the programming procedure. If only minor modifications are desired, the field pointer can be moved directly to the target field by pressing the appropriate cursor control keys.

The interactive fill-in-the-blank programming is further enhanced by the softkey concept. If the 4145A's operating system were controlled by a conventional keyboard, more than 200 keys would be needed, or the operator would have to input commands with alphabetic and numeric keys. The advantages of using softkeys are that an operator can quickly select the desired command from softkey prompts, and all possible commands and functions can be displayed. Thus, the operator doesn't have to memorize the commands or refer to a command summary or the manual.

Display Modes and Analysis Functions

Measurement results can be displayed in one of five different formats.

- Schmoo Plot (Fig. 8a). A three-dimensional (XYZ) display in which five level-dependent, weighted symbols indicate the relative values of measurement results on the Z-axis. The symbol at any selected X-Y measurement point can be highlighted by the cursor function to provide direct numeric readout of the Z-axis value.
- Matrix Display (Fig. 8b). A numerical presentation of a single characteristic affected by two varying parameters. For example, h_{FE} can be displayed as a function of base current I_B and collector-to-emitter voltage V_{CE}. The display can have up to 512 rows of data, corresponding to steps for variable VAR1, and up to six columns per row, corresponding to steps for the second variable VAR2. Matrix elements can be measured values or the results of user-function calculations.
- List Display (Fig. 8c). A complete numeric listing of up to six parameters and user-function results dependent on variable VAR1.
- Time Domain. The time dependency of semiconductor parameters can be observed and analyzed. This is done by not assigning VAR1 to any of the source channels (SMUs and voltage sources) on the CHANNEL DEFINITION page. Measurements over a period as long as 85 minutes can be made with measurement intervals specified from 10 ms to 10 s. Results can be displayed in graphic, matrix, or list formats.
- Graphic Display (Fig. 8d). The source variable, measurement variables (maximum of six) and user functions (maximum of two) can be independently assigned to three axes—X, Y1, and Y2. Therefore, two characteristics can be displayed simultaneously (double-Y-axis format). Various display scaling configurations can be specified independently of the sweep mode of the source variable (e.g., linear X-linear Y1-linear Y2, or linear-log-linear, or log-log-log).

The versatility of the graphics display mode is enhanced by its various analysis functions. The marker function pro-

[hp] *** CHANNEL DEFINITION ***

CHAN	NAME V	NAME I	SOURCE MODE	SOURCE FCTN
SMU1	VE	IE	V	VAR1
SMU2	VB	IB	COM	CONST
SMU3	VCE	IC	COM	CONST
SMU4				
Vs 1		-----	V	
Vs 2		-----	V	
Vm 1		-----	----	----
Vm 2		-----	----	----

USER FCTN	NAME (UNIT) = EXPRESSION
1	HFE ( ) = IC/IB
2	______( ) =

(a)

[hp] ****** SOURCE SET UP ******

	VAR1	VAR2
NAME	VE	
SWEEP MODE	LINEAR	LINEAR
START	.0000V	
STOP	-.9000V	-------
STEP	-.0100V	
NO. OF STEP	91	
COMPLIANCE	100.0mA	

CONSTANT	SOURCE	COMPLIANCE
VB COM	.0000V	105.0mA
VCE COM	.0000V	105.0mA

(b)

[hp] ** MEAS & DISP MODE SET UP **

MEASUREMENT MODE: SWEEP

DISPLAY MODE: GRAPHICS

	X axis	Y1axis	Y2axis
NAME	VE	IC	IB
SCL	LINEAR	LOG	LOG
MIN	.0000V	1.000pA	1.000pA
MAX	-1.0000V	100.0mA	100.0mA

(c)

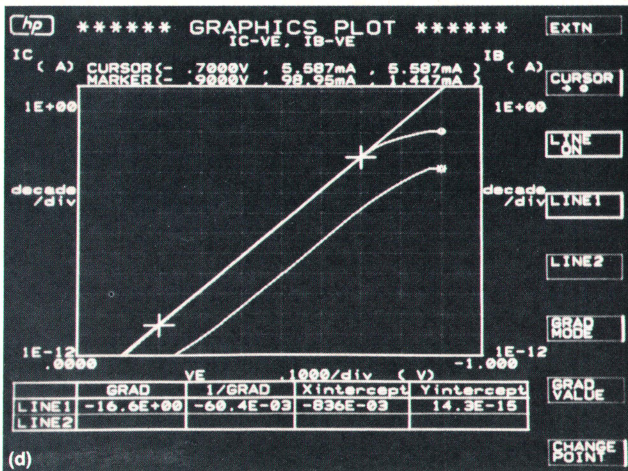

Fig. 7. *Typical measurement setup procedure for the 4145A. (a) CHANNEL DEFINITION page. The names and source modes for the SMUs are selected and the names of the voltage sources and monitors are specified. If required, the user functions are defined. (b) SOURCE SET UP page. The range of values and sweep modes are specified for each source. Delay and hold times can be specified by pressing the proper softkeys. (c) MEAS & DISP MODE SET UP page. The desired measurement and display modes are selected and the appropriate display variables are designated. (d) Typical graphics display for measurement setup example given in steps (a), (b), and (c).*

vides readout of not only measurement point values, but also intermediate point values by linear interpolation. The X, Y1, and Y2 coordinate values of any point on the graph can be read by the cursor function. The line function enables direct readout of slope (GRAD) plus X and Y intercepts.

Comparison functions are provided by the STORE and RECALL softkeys. They provide overlay displays or double-axis formats. The autoscale function optimizes graphic display scaling after measurement.

The zoom function horizontally or vertically expands (×2) or contracts (×0.5) the displayed graph. The zoom window can be moved to any location centered on the cursor. The background area of the vector memory can be used to display user-oriented graphics via the HP-IB. This function enhances user applications.

User Functions and Keyboard Arithmetic

The 4145A has two programmable user functions which provide real-time calculation of current-voltage dependent parameters, such as h_{FE}, g_m, and maximum-power hyperbola. All of the 4145A's arithmetic functions (+, −, *, /, √, EXP, LOG, LN, **, ABS, EEX, and Δ), variables (source and monitor names only), and physical constants (electron charge, Boltzmann's constant, and vacuum dielectric constant) can be used in the equation defining a user function. User functions are executed during measurements, and the calculation results can be displayed in the same manner as the measurement results. Keyboard calculations can be made at any time simply by keying in the expression and pressing **EXECUTE**. All of the arithmetic functions available for user-function definitions can be used. Also, keyboard calculations can be performed in conjunction with the display marker. For example, if the expression I_C/I_B is executed when the marker (indicated by the symbols • and *) is positioned at $V_E = -0.9V$ as shown in Fig. 7d, the value of the expression at this point will be displayed on the bottom line of the CRT (not shown in Fig. 7d).

Systems Use

The 4145A is equipped with the HP-IB, and almost all measurement functions are remotely programmable. Therefore, the 4145A is a powerful component for a semiconductor measurement system. For more sophisticated users, the 4145A has a special user mode. In this mode, an operator can control the SMUs, voltage sources and voltage monitors directly and use the CRT as an independent graphics plotter. The operator can use the powerful HP-GL commands and graphics utilities of HP's desktop computers to build a user-oriented dc parameter measurement system easily. The 4145A's **PLOT** function dumps all information displayed on the CRT directly onto a digital printer/plotter via the HP-IB, providing publication-quality hard copies. The plot area is front-panel programmable and no HP-IB controller is necessary. The **PRINT** function operates similarly, but only data stored in the measurement data buffer is printed. The external CRT output allows the operator to view test results on a large-screen monitor.

Small-scale systemization of the 4145A is possible by using an analog data link. For example, if you connect a capacitance meter equipped with an analog output to the

(a) ******* SCHMOO PLOT *******

Zaxis = HFE

(b) ****** MATRIX DISPLAY ******

VCE = .0000V to 1.0000V in .0100V step
IB = 10.00μA to 50.00μA in 10.00μA step

[HFE MEASUREMENT]

VCE	IB 10.00μA	20.00μA	30.00μA
.0000V	-1.08E+00	-1.06E+00	-1.07E+00
.0100V	2.75E+00	3.03E+00	3.22E+00
.0200V	8.12E+00	8.66E+00	9.02E+00
.0300V	15.7E+00	16.5E+00	17.0E+00
.0400V	25.8E+00	26.7E+00	27.1E+00
.0500V	39.4E+00	40.2E+00	40.0E+00
.0600V	56.8E+00	56.5E+00	55.5E+00
.0700V	78.1E+00	76.2E+00	73.5E+00
.0800V	103E+00	98.4E+00	93.3E+00
.0900V	132E+00	123E+00	115E+00

(c) ******* LIST DISPLAY *******

VCE = .0000V to 1.0000V in .0100V step
IB = 10.00μA to 50.00μA in 10.00μA step [10.00μA]

VCE	IE	VB	IC
.0000V	-88.90nA	.5890V	-9.988μA
.0100V	-37.21μA	.5990V	27.44μA
.0200V	-90.86μA	.6080V	80.85μA
.0300V	-166.3μA	.6180V	156.6μA
.0400V	-268.4μA	.6270V	258.4μA
.0500V	-404.4μA	.6350V	394.3μA
.0600V	-576.3μA	.6430V	566.5μA
.0700V	-790.7μA	.6510V	780.8μA
.0800V	-1.042mA	.6570V	1.032mA
.0900V	-1.326mA	.6630V	1.316mA

(d) ****** GRAPHICS PLOT ****** TEMPERATURE TRANSIENT

Fig. 8. *Examples of display formats available on the 4145A digital CRT display. (a) Schmoo plot of h_{FE} versus I_B and V_{CE}. (b) Matrix display of data used in (a). (c) List display of I_E, V_B, and I_C versus V_{CE} at I_B = 10.00 μA. (d) Graphics plot of h_{FE} versus time (temperature transient).*

4145A, you can plot the C-V curve of a device on the 4145A's CRT. In such a measurement, one SMU stimulates the device under test, which is connected to the capacitance meter. The analog output of the capacitance meter is connected to another SMU or a voltage monitor which measures the analog voltage. The 4145A's user functions can then calculate and display the capacitance values. By using the appropriate transducer, you can also handle other physical parameters such as temperature and pressure.

Fig. 9 is an example of a 1-MHz C-V measurement and a quasistatic C-V measurement made by a system consisting of the 4145A, HP 4140B pA Meter/DC Voltage Source and HP 4271B 1 MHz Digital LCR Meter.

Autosequence Programs

The 4145A can be programmed to perform sequential measurements and output the results. The autosequence setup shown in Fig. 10 is an automated procedure for measuring the I_C, I_B-V_{BE}, h_{FE}-I_C, I_C-V_{CE} and V_{CE}(SAT) characteristics of a bipolar transistor. The autosequence program initiates a measurement sequence, activates the plotter/printer for hard-copy results and then stores the

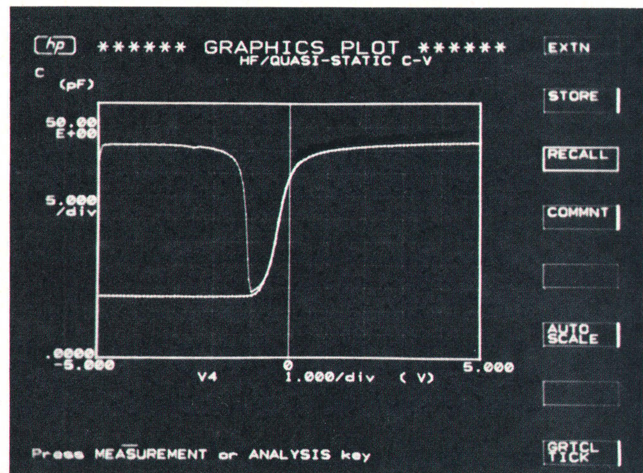

Fig. 9. *Sample display of C-V data obtained with the 4145A and an external capacitance meter and picoammeter/dc voltage source. The upper curve is the quasistatic capacitance data and the lower curve is the high-frequency (1 MHz) capacitance data.*

```
*** AUTO SEQUENCE SET UP ***

 1  GET P  ICBVBE                    Call up program from disc
 2  SINGLE                           Single sweep
 3  PLOT   100, 3600, 3500, 7000     Output CRT display contents to plotter
 4  SAVE D ICBVBE                    Save test results on disc
 5  GET P  HFE1
 6  SINGLE
 7  PLOT   100, 100, 3500, 3500
 8  GET P  NPN1
 9  SINGLE
10  PAUSE                            Allows viewing of results before output to plotter
11  PLOT   3600, 3600, 7000, 7000
12  GET P  VCESAT
13  SINGLE
14  PLOT   3600, 100, 7000, 3500
15  PAGE                             Advance plotter page
16  WAIT   60                        Wait time before execution of next command
17  PRINT
18
19
20
21
22
23
24
```

Fig. 10. *A typical autosequence program for the 4145A. This feature allows a user to develop measurement setups, save them by name on the internal disc unit, and then later call them back in any order automatically, including plotting and saving any results.*

measurement data on the flexible disc.

Test Fixture

The 16058A Test Fixture (Fig. 11) is furnished with the 4145A. The 16058A holds the device to be tested and provides all necessary connections to the test input/output terminals of the 4145A. For stable and accurate measurements at extremely low current levels, the 16058A is furnished with an electrostatic light-shielding cover. This cover is also a safety feature to protect users from hazardous voltages. When the cover is open, output voltages are limited to 42 volts automatically. To facilitate testing various types of devices, eight interchangeable socket boards and three types of special plug leads are furnished.

Acknowledgments

The authors wish to thank Hiroshi Kanamori and Hideyuki Hasegawa for developing the digital hardware and software, Akinori Maeda for power supply design, Yoshimasa Shibata for mechanical design, Tsuneji Nakayasu and Akihiko Goto for test fixture and industrial

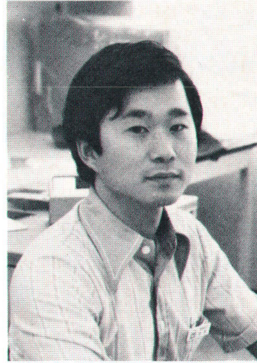

Jin-ichi Ikemoto

Jin-ichi Ikemoto received the BS (1972) and MS (1974) degrees in electrical engineering from Waseda University. With Yokogawa-Hewlett-Packard since 1974, he has worked on automatic test systems in the computer group for about three years. Since joining the R&D lab, he has contributed to the design of the 4191A RF Impedance Analyzer and designed the main processing, HP-IB, and mass storage sections of the 4145A. Jin-ichi is single and enjoys playing the guitar and swimming.

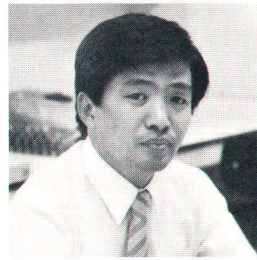

Fumiro Tsuruda

Fumiro Tsuruda was born in Kagoshima, Japan, and received his BSEE and MSEE degrees from Tokyo Institute of Technology in 1972 and 1974. He joined Yokogawa-Hewlett-Packard in 1977, and worked on the 4140B pA Meter/Voltage Source and designed the digital section of the 4145A, mainly the software. He enjoys playing the guitar and the recorder.

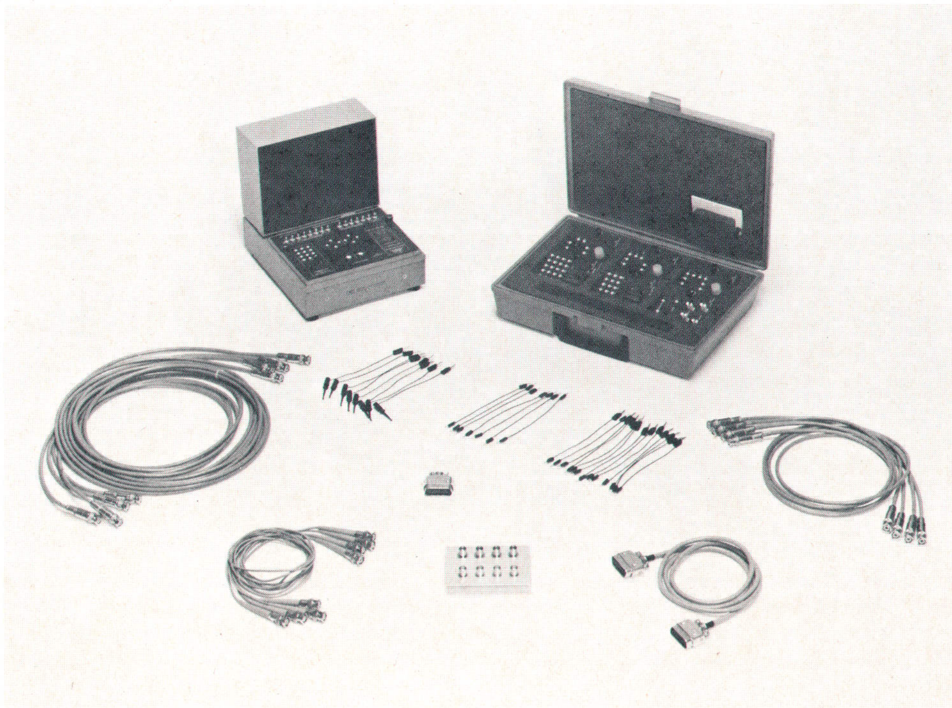

Fig. 11. *Each 4145A comes complete with the HP 16058A Test Fixture, cables, and connector plates. Also included (not shown) are five system discs and a head cleaning disc.*

Kohichi Maeda
Kohichi Maeda received his MSEE from Waseda University, Tokyo, in 1963. Since joining Yokogawa-Hewlett-Packard in 1964, he has worked on the 4271A 1-MHz Digital LCR Meter, the 4261A LCR Meter and the 4274A/4275A Multi-Frequency LCR Meter. He served as project manager for the 4145A. Kohichi and his wife have three children. Playing tennis is his main recreation.

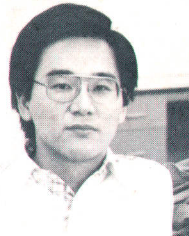

Teruo Takeda
Teruo Takeda received his BSEE and MSEE degrees from Waseda University in 1976 and 1978, respectively. He joined Yokogawa-Hewlett-Packard in 1978, and was responsible for the design of the ADC, DAC, and the SMU controller of the 4145A. He transferred to HP's Stanford Park Division this past June to attend Stanford University. He's married, and enjoys working on audio equipment and singing.

design, and Kazunori Nishitsuru and Hideyuki Norimatsu for application evaluation. We would like to express our appreciation to Ulrich Kaempf of HP's Integrated Circuit Processing Laboratory who introduced us to the SMU concept. Special thanks are also due Haruo Ito, our section manager, who gave us the original idea of the product and many useful suggestions. To many other people not mentioned here who contributed to the product's development, many thanks.

Reference:

1. K. Hasebe, W.R. Mason, and T.J. Zamborelli, "A Fast, Compact High-Quality Digital Display for Instrumentation Applications," Hewlett-Packard Journal, Vol. 33, no. 1, January 1982.

Programmable Stimulus/Measurement Units Simplify Device Test Setups

by Susumu Takagi, Hiroshi Sakayori, and Teruo Takeda

EVALUATION OF SEMICONDUCTOR DEVICES and materials requires an assortment of dc current and voltage sources and monitors. To connect these to the device or material to be tested usually requires an array of cables and a matrix of switches. As such, setting up the equipment for a particular measurement is often complicated and time-consuming. In addition, the nest of cables and the switch contacts can contribute significant resistance, capacitance, inductance, and electrical noise components that adversely affect measurement accuracy and speed. To minimize these problems and simplify test setups, a new approach was chosen for the HP 4145A Semiconductor Parameter Analyzer—the use of programmable stimulus/measurement units (SMUs).

Stimulus/Measurement Unit

Each of the four stimulus/measurement units in the 4145A is an independently adjustable, analog-voltage-controlled dc port that can be programmed from the 4145A's front panel or via the HP-IB* to function either as a voltage source and current monitor (V mode), as a current source and voltage monitor (I mode), or as a ground reference (COM mode). Also, each SMU can be programmed to increment or sweep its output.

*Hewlett-Packard Interface Bus, HP's implementation of IEEE Standard 488 (1978).

The main advantage of programmable SMUs is that a device can be completely characterized using only one setup. For example, a transistor can be characterized in common-base, common-collector, and common-emitter configurations without having to change the physical connections between it and the 4145A.

Design Considerations

In designing the 4145A's SMUs, two approaches were considered: a basic voltage source capable of limiting output current and a basic current source capable of limiting output voltage. The dc characteristics shown in Fig. 1a are those of a basic current-limiting voltage source. This voltage source operates in the current-limit mode when the voltage setting results in an output current that exceeds the preset limits. In this mode, the voltage source now behaves like a current source. In Fig. 1a, two different loads are shown: R_{L1} and R_{L2}. R_{L1} is relatively high, forcing the source into a constant-voltage mode, and R_{L2} is relatively low, forcing the source into a current-limited mode.

The dc characteristics shown in Fig. 1b are those of a basic current source capable of voltage limiting. There is no difference between the two types of sources in normal operation. In the limited operation region, however, there is a great difference. The voltage source just needs to increase

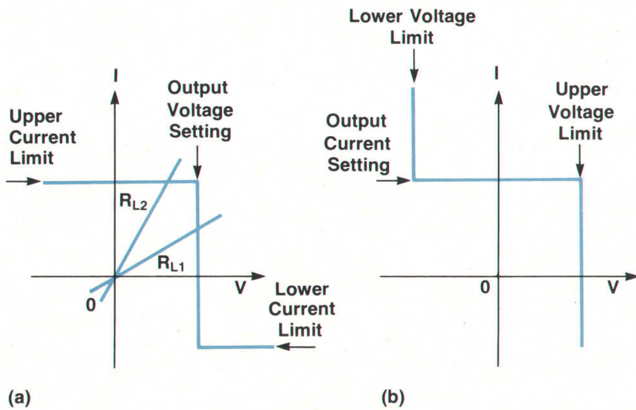

Fig. 1. *(a) Output characteristic of a current-limited voltage source. (b) Output characteristic of a voltage-limited current source. This source is impractical for real designs because of the inability to supply very large currents at the voltage limit.*

the output voltage until the current limit is reached. However, the current source must be able to clamp the output voltage with an infinite current source or sink capability. In real applications, such abnormal conditions can occur when the current source is incorrectly programmed or when the connections between its outputs and the pins of the device under test (DUT) are incorrect. This capability for infinite current is not feasible in practical designs, and it can easily damage the load or device under test.

There were two other considerations in designing the SMUs. One was to obtain stable operation of each SMU independent of the other SMUs and the DUT's characteristics. The other was to prevent excessive SMU output voltage that could result in damage to a sensitive DUT. One of the keys to stable SMU operation is the novel guard filter scheme. This will be discussed later.

Most circuit designers have observed a partial or total loss of h_{FE} for transistors operating in the low-collector-current region. This is often caused by voltage transients. For example, a transient spike exceeding 25 mV can totally change the characteristics of some sensitive semiconductor devices. Some of the methods used in the 4145A to suppress undesirable excessive output voltages are implemented in the SMU hardware. But much of the suppression is in the firmware in the ROMs of the SMU controller. This spike suppression is effective even at instrument power on/off.

Construction

A simplified block diagram of an SMU is shown in Fig. 2. Only one of the three error amplifiers controls the power amplifier during normal operation. The other two error amplifiers operate in their standby mode and take control when the output compliance is reached. The SMU output voltage V_o is buffered by the voltage follower and fed back to the voltage error amplifier. It is measured by the voltage monitor amplifier which normalizes it to the analog-to-digital converter (ADC) input level. The SMU's output current develops a proportional voltage across the selected range resistor which is measured by the current monitor amplifier after the unwanted common-mode voltage error is rejected. The output of the current monitor amplifier is also

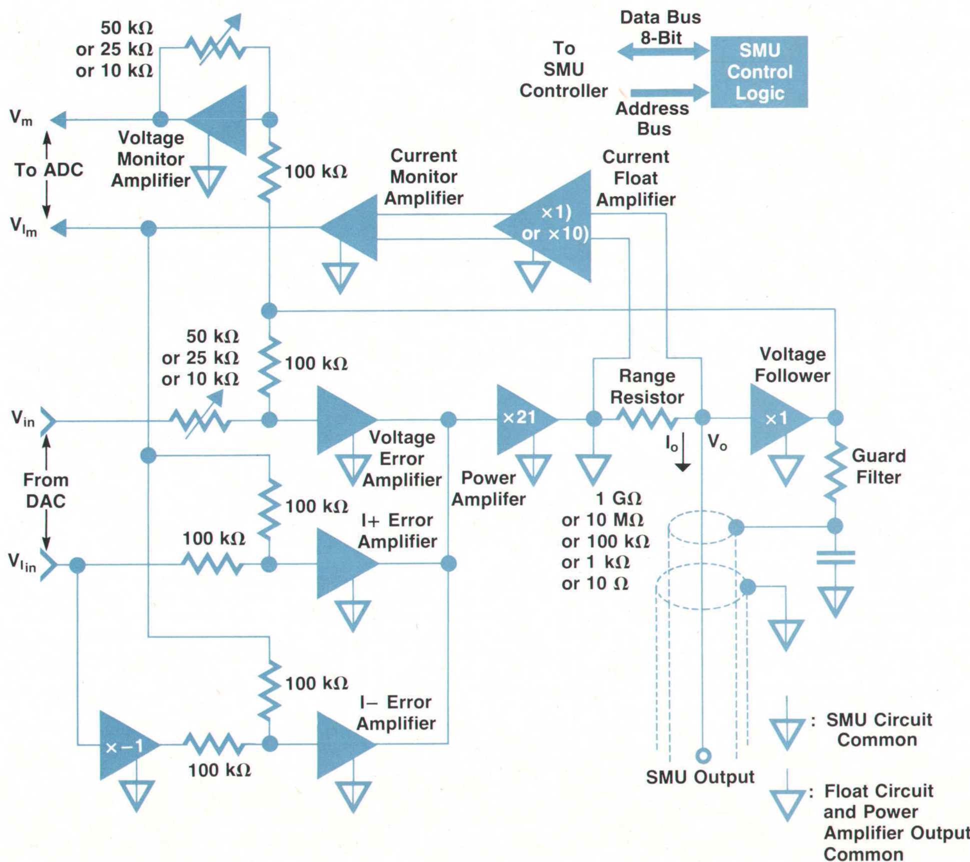

Fig. 2. *Simplified block diagram of one of the four SMUs used in the 4145A Semiconductor Parameter Analyzer.*

normalized to the ADC input level and fed back to the I+ error amplifier and the I− error amplifier. Five range resistors and the selectable gain factor (×1 or ×10) of the current float amplifier provide the wide output current range (1 pA to 100 mA) of the SMU with excellent accuracy.

The connection of the SMU output to the DUT is made by a triaxial cable whose inner shield is connected to the voltage-follower output so that it surrounds the center conductor with an equipotential field. The outer shield is connected to the low-impedance circuit common. This configuration effectively prevents the SMU output's picking up undesired noise. This is particularly important in low-current measurements, where the noise level can exceed the signal level by several decades.

Guard Filter

The guard filter is a novel approach implemented in the 4145A SMUs. It contributes greatly to stable, oscillation-free SMU operation, especially in the very-low-current ranges. Fig. 3 shows a simplified schematic of the output circuit of the SMUs and the equivalent circuit.

The guard capacitance C_g consists mainly of the capacitive coupling between the center conductor and inner shield (guard) of the triaxial cable. Y_I' and Y_x' in Fig. 3b represent the additional admittances of C_g that appear in parallel with the range resistor R_I and the load R_x, respectively. In equation form:

$$Y_x' = j\omega C_g[1-F(\omega)] \quad (1)$$

$$Y_I' = j\omega C_g[F(\omega)/(1+A_v)] \quad (2)$$

where $F(\omega)$ is the transfer function of the guard filter and A_v is the open-loop gain of the voltage follower, whose power supply is referenced to the power amplifier output.

When the guard is connected directly to the voltage follower output, $F(\omega)$ equals 1, and equations (1) and (2) become

$$Y_x' = 0 \quad (3)$$

$$Y_I' = j\omega C_g/(1+A_v) \approx j\omega C_g/[1+(2\pi f_T/j\omega)] \quad (4)$$

where f_T is the gain-bandwidth product of the internally compensated voltage follower. At frequencies much less

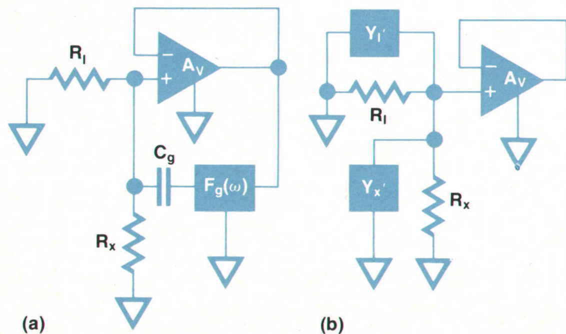

Fig. 3. *(a) Simplified schematic of guard filter. (b) Equivalent circuit for (a).*

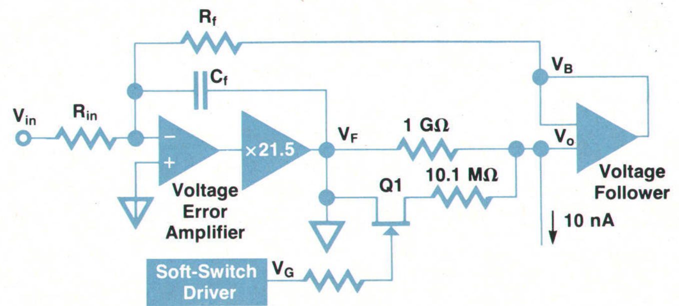

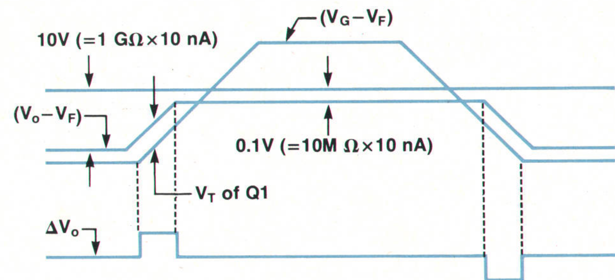

Fig. 4. *(a) Schematic of soft-switching circuit for current ranging with negligible effect on the output voltage. (b) Voltage relationships for circuit shown in (a) during a range change.*

than f_T:

$$Y_I' \approx -\omega^2 C_g/2\pi f_T \quad (5)$$

The total range admittance $Y=(1/R_I)-Y_I'$ becomes negative for frequencies above 500 Hz, given a range resistance of 1 GΩ, guard capacitance of 500 pF and f_T of 1 MHz, for instance. This means that the feedback component of the output current is not negative but positive above 500 Hz. This indicates that stable SMU operation totally free from oscillation is not possible without changing parameters that would sacrifice SMU performance (speed, resolution, et cetera).

The simple low-pass guard filter provides the solution without degrading SMU performance. At frequencies above the cutoff frequency f_L of the low-pass filter, Y_I' and Y_x' are approximated as follows, on the condition that $f_L << f_T$:

$$Y_I' = j\omega C_g\left(\frac{1}{1+j\omega/2\pi f_L}\right)\Big/\left(1+\frac{2\pi f_T}{j\omega}\right) \approx j\omega C_g\left(\frac{f_L}{f_T}\right) \quad (6)$$

$$Y_x' = j\omega C_g\left(1-\frac{1}{1+j\omega/2\pi f_L}\right) = j\omega C_g\left(\frac{j\omega/2\pi f_L}{1+j\omega/2\pi f_L}\right) \approx j\omega C_g \quad (7)$$

Thus, with the guard filter, the additional admittance becomes a capacitance of $C_g(f_L/f_T)$ without a negative resistance and only the feedback of the output current component lags at high frequencies. Moreover, the additional capacitance C_g, which appears in parallel with the load, contributes to stability in the current-control mode.

The low-pass characteristics of the guard filter also function to surround the center conductor of the triaxial cable with an equipotential surface.

Current Ranging

Current ranging in each SMU is performed automatically so that optimum accuracy is assured. This requires a spikeless current-range change scheme to prevent sudden changes of output voltage during a range change that can adversely affect a sensitive DUT.

A novel soft-switch scheme, shown in Fig. 4, is used in the 4145A to control current ranging. By turning Q1 on or off, a range resistance of 10 MΩ or 1 GΩ can be selected. To maintain the SMU output current at 10 nA when switching range resistance from 1 GΩ to 10 MΩ, the voltage across the range resistor (V_o-V_F) must change between +10V and +0.1V as shown in Fig. 4. The maximum change rate of V_F versus time is determined by the response of the voltage control loop. The range resistance value cannot change faster than the response of the voltage control loop without causing a transient change in V_o. This is prevented by applying to the gate of Q1 a ramp voltage V_G whose slew rate is slow enough to allow V_F to change in step with the change in range resistance.

During this change, the output voltage V_o is kept nearly constant by the voltage error amplifier. However, a small

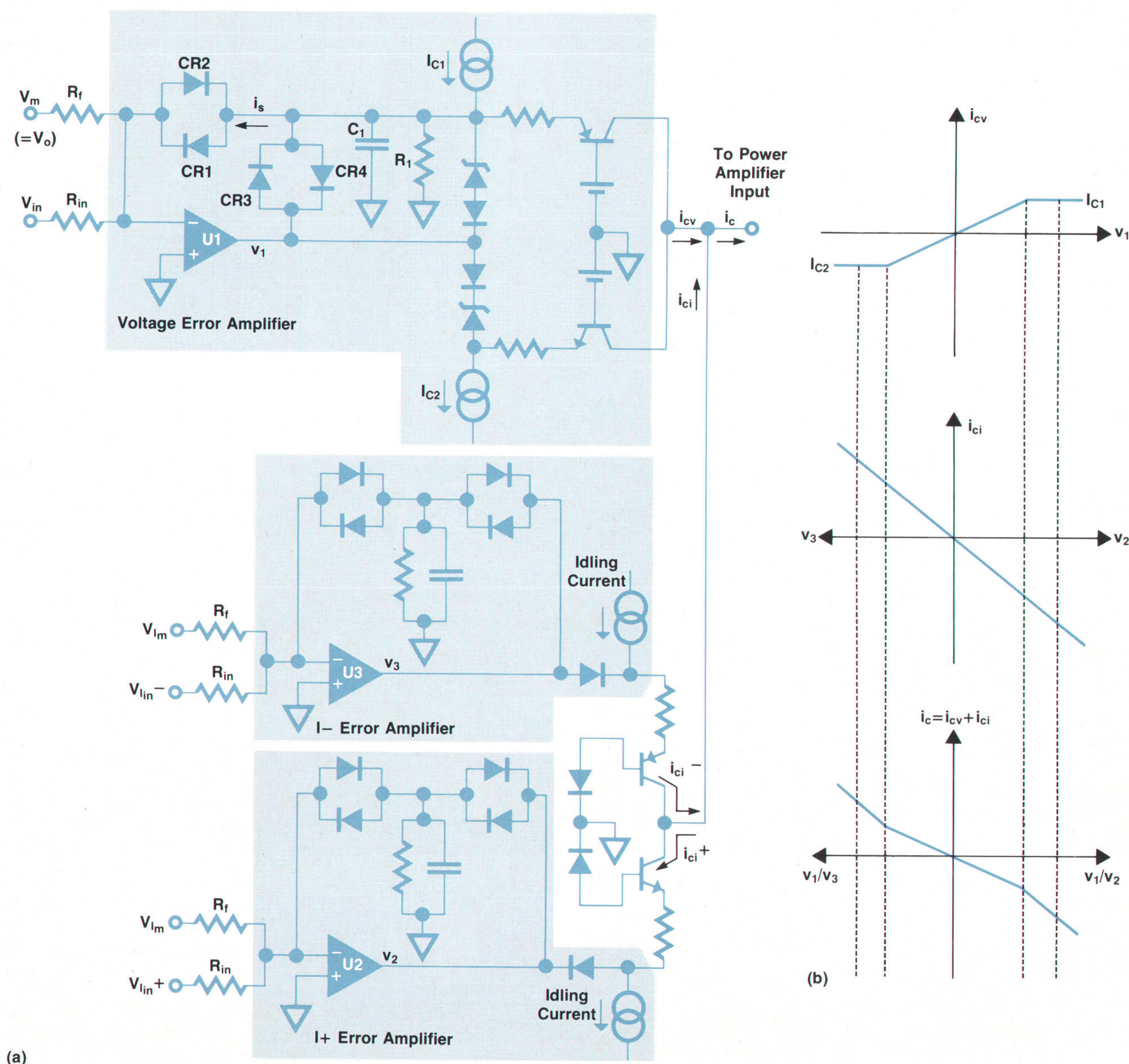

Fig. 5. *(a) Schematic of the SMU voltage and current control amplifiers. (b) Output characteristics of the voltage and current control amplifiers.*

amount of output voltage disturbance is required to supply the feedback loop current to change V_F as calculated by

$$\Delta V_o = -\frac{dV_F}{dt}(C_fR_f) = -\left(\frac{dV_F}{dt}\right)\frac{1}{2\pi f_v} \quad (8)$$

where f_v is the total gain-bandwidth product of the voltage control system. In the 4145A the gain-bandwidth product of the SMUs is 200 kHz and the ramp rate of the soft switches is 5V/ms. Thus, ΔV_o is only 4.0 mV.

The ramp signal is referenced to V_G or V_o, whichever is more positive, so that a single n-channel FET can handle the slew-rate-limited current ranging for both directions of output current.

The current range, which is selectable simply by changing the gain of the current float amplifier (Fig. 2) from ×1 to ×10, requires no special circuitry. During current ranging, a control signal called I Loop Cut is fed back to the I+ and I− error amplifiers to inhibit their override capability and ensure SMU control by the voltage error amplifier. When I Loop Cut is enabled, the other changes inherent to the current ranging, such as the analog input which must be changed to correspond with the new range factor, are done in a predetermined manner by the SMU controller. If the SMU is operating in a current-control mode before the change, the input reference voltage V_{in} is modified step by step until the SMU reaches its voltage-control mode. At the instant of detecting the SMU control mode change, the I Loop Cut signal is asserted and V_{in} is held constant so that the current ranging is done at the same (actually a little less in magnitude) output current.

Control-Mode Change

Each SMU has three control amplifiers. They are the voltage error, I+ error and I− error amplifiers and the control modes they monitor are called the V control mode, I+ control mode and I− control mode, respectively. One of them is selected in accordance with the input reference voltage and feedback signal levels. In each of the SMU control modes the error amplifiers not used are completely out of the control loop and do not affect operation. However, they are in a standby condition, ready to take over SMU control at the instant that the feedback level to any standby error amplifier is about to exceed its input reference.

Fig. 5 shows a simplified schematic of the voltage, I+, and I− error amplifiers and their output characteristics. The construction of the I+ and I− error amplifiers is almost identical to that of the voltage error amplifier except that the values of the current sources are appropriate to overridable and one-sided control, and their outputs are connected to that of the voltage error amplifier. All three are connected to the input of the power amplifier, which develops the specified output voltage or current to the load through the range resistor.

When v_1 (output of U1) is near zero, the voltage error amplifier controls the total loop so that the output voltage is proportional to V_{in} and the SMU works in its voltage-control mode. v_1 varys from near-zero to maintain the desired output voltage until it reaches a level equal to two diode forward-voltage drops. At this time a current i_s flows in the internal feedback loop of the voltage error amplifier and it can no longer control the SMU output voltage. Then control by the I+ or I− error amplifiers is established and the SMU's output current is proportional to the voltage $V_{I_{in}}$ to the I+ and I− error amplifiers.

The voltage error amplifier U1 is not saturated at this time, but is operating with a local feedback current i_s to prevent saturation of the voltage control loop and v_1 is set near its control level by twice the diode forward-voltage drop.

From another point of view, as long as the saturation-prevention current is maintained, the voltage error amplifier is kept ready to control and maintain the SMU output voltage. All error amplifiers work to maintain the present output condition. Thus the smooth transfer of control modes during changes in settings and outputs of the SMU is assured, preventing overshoot or spikes at the output.

Automatic Calibration

The monitor functions of the SMU can be used for self-calibration. Output errors can be compensated by measuring the raw errors with the calibrated monitors. All offset errors of the SMU source/monitor are updated every five minutes by the normal measurement sequence. Extensive use of high-stability precision resistors and resistor networks in the SMU design eliminates the need for gain adjustments. Because only the single high-performance DAC and the single high-performance ADC are used to communicate between all of the SMUs and the SMU controller, no individual adjustments are required for each SMU.

Stability

The dc characterization of semiconductors is sometimes affected by oscillation. There are two modes of oscillation, one caused by the SMU, and the other caused by the DUT and the connection leads. The oscillation caused by the SMU occurs when an inductive load is connected to the SMU output. The oscillation frequency is low, less than 300 kHz. The SMU often has an inductive load because the output impedance of the SMU is inductive in V-mode operation and usually several SMUs are connected to each other through the DUT.

There are two sources of SMU oscillation, one related

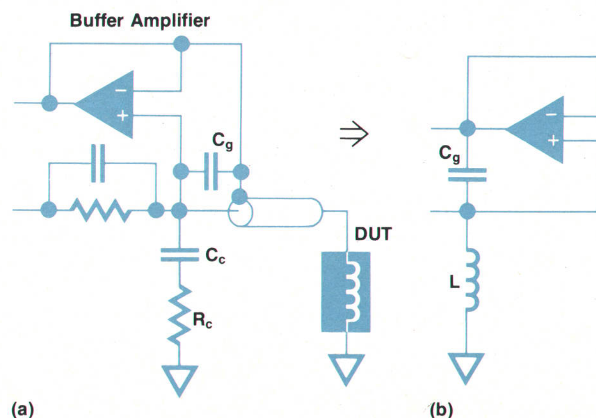

Fig. 6. *(a) SMU output circuit. (b) Equivalent circuit for (a).*

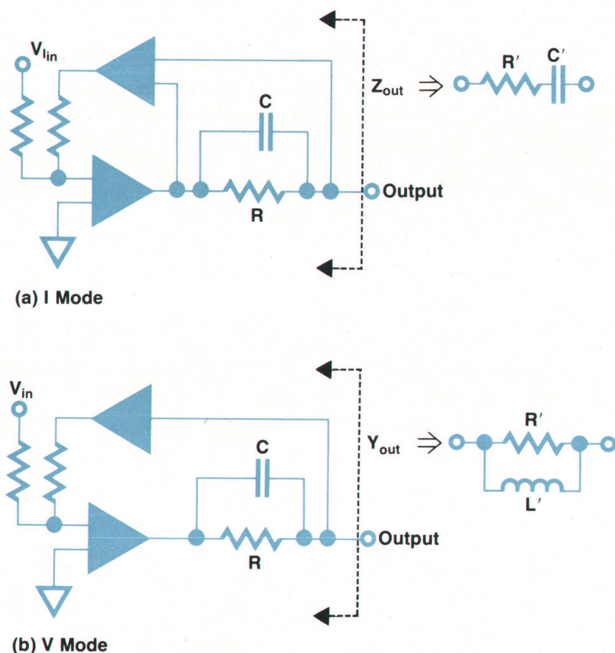

Fig. 7. *(a) Output impedance circuit of SMU in the I mode. (b) Output admittance circuit of SMU in the V mode.*

solely to the output stage of the SMU and the other related to overall SMU construction when operating in the I mode (current forcing and voltage sensing). Fig. 6a shows a simplified drawing of the SMU output circuit. Here, C_g is the capacitance between the center conductor and the inner shield of the triaxial output cable. Redrawing Fig. 6a, we obtain Fig. 6b. If the Q of the C_g-L circuit exceeds unity, this circuit will oscillate at a frequency of $1/2\pi\sqrt{C_gL}$. Fig. 7a shows the equivalent circuit of an SMU operating in the I mode. The output impedance of this circuit (Z_{out}) is.

$$Z_{out} = \frac{R(1-\omega_oCR)}{1+(\omega CR)^2} + \frac{R(\omega^2CR+\omega_o)}{j\omega\left[1+(\omega CR)^2\right]} \quad (9)$$

where ω_o is the resonant frequency of the system consisting of two amplifiers. Thus, if $\omega_oCR>1$, the equivalent series resistance of Z_{out} is negative. If an inductive load is connected that cancels the equivalent series capacitance of Z_{out}, this system will oscillate.

What is the chance of being connected to an inductive load? When the SMU is operating in the V mode (voltage sourcing and current sensing), the output impedance of the SMU is inductive (Fig. 7b). When an inductance L is connected to the emitter of a transistor, its effect is multiplied because the base input impedance of the transistor is L times h_{fe}. Fig. 8 depicts another example. The SMUs connected to the MOSFET's gate and drain are operating in the V mode, so these SMUs appear to be inductive, making this configuration equivalent to a Hartley oscillator.

To prevent oscillation, the SMU uses a network consisting of C_c and R_c as shown in Fig. 6a to compensate for the output inductive reactance. However, the value of C_c cannot be made large enough to make Z_{out} capacitive because of the need of a short settling time. Therefore, the SMU may

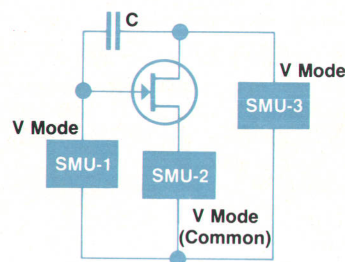

Fig. 8. *A test configuration that could cause SMU oscillation. It is equivalent to a Hartley oscillator because SMUs operating in the V mode can act as inductive components.*

oscillate if an unusually large inductance is connected. This can occur when the DUT is a high-h_{fe} (>3000) transistor and the SMU connected to its emitter is set to a low-current range. If oscillation does occur, it is detected by the oscillation detector in the 4145A and an error message is displayed on the 4145A's CRT.

The second source of oscillation does not depend on the structure of the SMU, but on the combination of the DUT and stray parameters around the DUT, such as load inductance and parasitic capacitance. The frequency of this type of oscillation is rather high, well into the 3-to-30-MHz region. This type of oscillation usually cannot be detected by the 4145A's oscillation detection circuit. To prevent oscillation, we can use ferrite beads on the test leads. If an unusual display appears, we recommend the use of additional ferrite beads on the DUT leads.

Hiroshi Sakayori

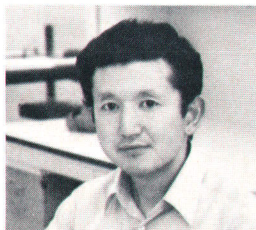

Hiroshi Sakayori earned his BS degree in electrical engineering from Waseda University in 1972 and joined Yokogawa-Hewlett-Packard the same year. He helped design the SMU and developed the analog performance test system for the 4145A. He enjoys mountain climbing, skiing and watching Noh plays in his spare time.

Susumu Takagi

Susumu Takagi earned his BS degree in electrical engineering from Kyoto University in 1970. He joined Yokogawa-Hewlett-Packard the same year as a design engineer. He has worked on the 1504A/1505A Electrocardiograph and the 4140A pA Meter/DC Voltage Source. He designed the SMU of the 4145A. Susumu and his wife have two sons. He enjoys camping, woodworking and assembling models of various kinds.

HQMOS: A High-Performance NMOS Technology

Innovative processing methods are used to fabricate a scaled-down version of a standard n-channel MOS process, resulting in lower power consumption and higher speed.

by Horng-Sen Fu, Roger To-Hoi Szeto, Anders T. Dejenfelt, and Devereaux C. Chen

SEMICONDUCTOR DEVICE TECHNOLOGY is one of the most rapidly changing technologies in modern society. Among major semiconductor device technologies, such as bipolar, MOS (metal-oxide-semiconductor), and III-V or II-VI compounds, MOS has probably advanced the fastest in recent years, especially during the past decade. Silicon processing technology, on which most bipolar and MOS devices are based, has emerged as a major manufacturing technology mainly because of the ability to grow high-quality silicon dioxide. This greatly reduces device fabrication difficulty. Although III-V and II-VI compound technologies have made major progress in recent years, they still cannot compete with silicon technology because of material preparation and device fabrication problems.

Bipolar devices have been traditionally recognized as superior to MOS devices in speed because of fundamental differences in device structure and operating principles. This tradition has changed recently because of advances in MOS processing that now allow MOS to achieve a faster access speed than its bipolar counterpart.

Back in 1969, the standard MOS fabrication technology was an aluminum-gate p-channel process that exhibited low device density and slow speed compared to today's MOS circuits. A major breakthrough was the realization of self-aligned silicon-gate processing. This greatly reduced the parasitic overlap capacitance between an MOS device's gate electrode and its source and drain, thus achieving more speed and improving circuit performance.

Because electron mobility in silicon is higher than hole mobility, n-channel MOS devices are faster than p-channel MOS devices using today's shorter device channel lengths. The use of n-channel technology and the introduction of the depletion-mode device as an active load were two other steps toward high-speed MOS devices. Perhaps the most recent advance in MOS circuit performance has been the development of device scaling theory.[1] Reducing the size of an MOS device gains the advantages of shorter propagation

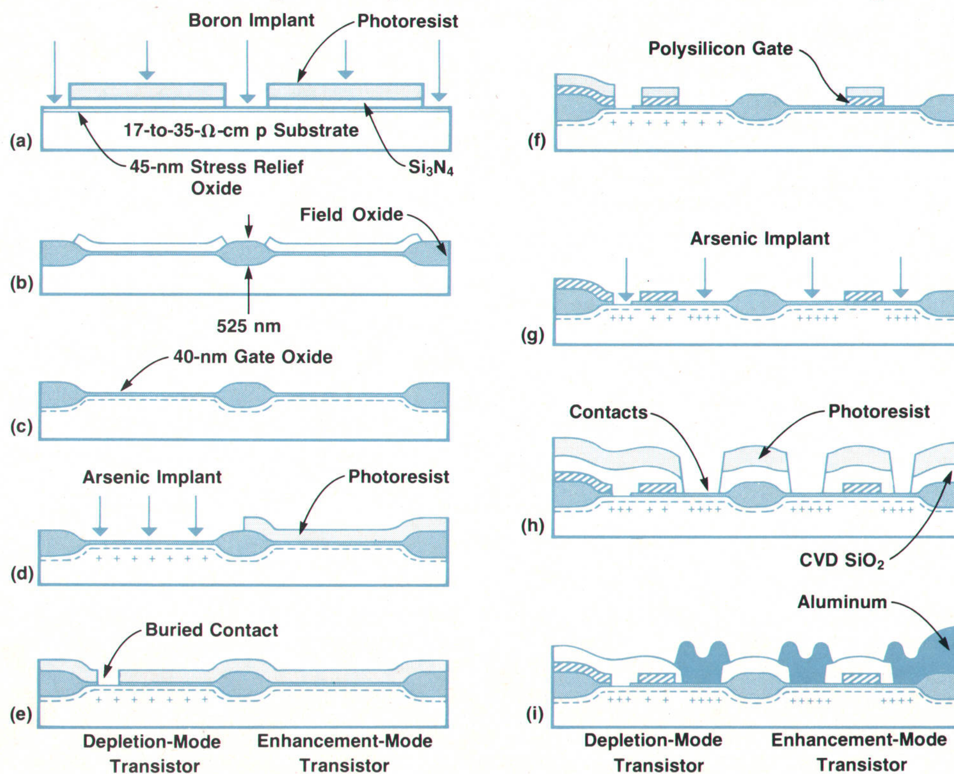

Fig. 1. *HQMOS process sequence. (a) Boron field implant threshold-voltage adjustment. (b) After field oxidation. (c) After gate oxidation. (d) Arsenic depletion implant. (e) After buried contact etch. (f) After polysilicon gate definition. (g) Arsenic source-drain implant. (h) After contact oxide etching. (i) Completed structure before final passivation step.*

delay and lower power dissipation without losing the basic operating characteristics of its original size. If the feature size (linewidth) is shrunk by a factor k (k>1), then the propagation delay is divided by k, power dissipation by k^2, and delay-power product by k^3. Thus it is possible to achieve high-speed, low-voltage MOS operation that competes directly with bipolar devices.

HQMOS Process

The HQMOS process is a scaled-down version of a standard n-channel MOS process. Because the feature sizes are smaller, new patterning and etching techniques are required. For example, polysilicon gates, contacts, and aluminum lines are formed by state-of-the-art dry-etching processes. A 10:1 optical projection wafer stepper and mask aligner and a positive photoresist process are also needed for all photomasking levels to define the narrow lines and spacings. Several innovative processing techniques, such as a new buried contact scheme for thin gate insulators,[2] a three-step contact etching process, and a low-temperature steam process to flow phosphorus-doped oxide were developed and implemented. Fig. 1 shows the major processing and masking steps of the HQMOS process, with the exception of the seventh and final masking step that defines the windows through the top passivation layer to the metal bonding pads.

Because junction and line capacitances are major factors contributing to circuit delay, it is important that parasitic capacitances be kept to a minimum. A lightly-doped silicon substrate helps reduce junction capacitance. HQMOS substrate material is p-type, has a <100> surface orientation, and has a resistivity of 17 to 35 ohm-cm. This corresponds to a boron doping level of 4 to $8\times10^{14}/cm^3$. A boron implant is required to adjust the threshold voltage of the MOS transistors and to prevent source-to-drain punchthrough. This implant is done before the polysilicon deposition and is subject to all subsequent heat treatments. A thin layer of stress-relief oxide, approximately 45 nm thick, is grown first on the fresh surface of the starting wafer. A 150-nm-thick film of high-quality silicon nitride is deposited on top of the stress-relief oxide. A 1.1-μm-thick layer of positive photoresist is applied and patterned by photolithographic means to define the active device regions. CF_4/O_2 plasma is used to etch the nonmasked silicon-nitride areas. A boron implant dose of $2\times10^{12}/cm^2$ at 70 keV is used to adjust the threshold voltage of the field regions. A cross section of the device structure at this point is shown in Fig. 1a. The next step grows about 525 nm of field oxide in a 900°C steam ambient using silicon nitride to mask the active regions (Fig. 1b). The nitride layer is then removed by a hot phosphoric acid etch. An enhancement-threshold-voltage-adjustment boron implant is done at this stage with a dose of $7\times10^{11}/cm^2$ at 50 keV. The stress-relief oxide is etched off and a fresh layer of oxide about 40 nm thick is regrown on the surface of the active regions as shown in Fig. 1c. Now depletion-threshold-adjustment masking and an arsenic implant can be done selectively on those regions where depletion transistors will be built as shown on the left side of Fig. 1d. This step can be repeated for different arsenic implant energies and doses on different regions depending on the needs of the circuits. The next step, which is optional, opens buried contacts for the depletion-mode transistors. A new buried contact process was developed and used here to avoid the gate oxide degradation problem encountered in a conventional buried contact process. A more detailed description of this new process will be given later. Fig. 1e shows the device cross section after the contact oxide is etched. A 400-nm-thick layer of polysilicon is deposited on the surface using a low-pressure chemical-vapor-deposition (LPCVD) process, and is doped with phosphorus using a standard $POCl_3$ predeposition cycle.

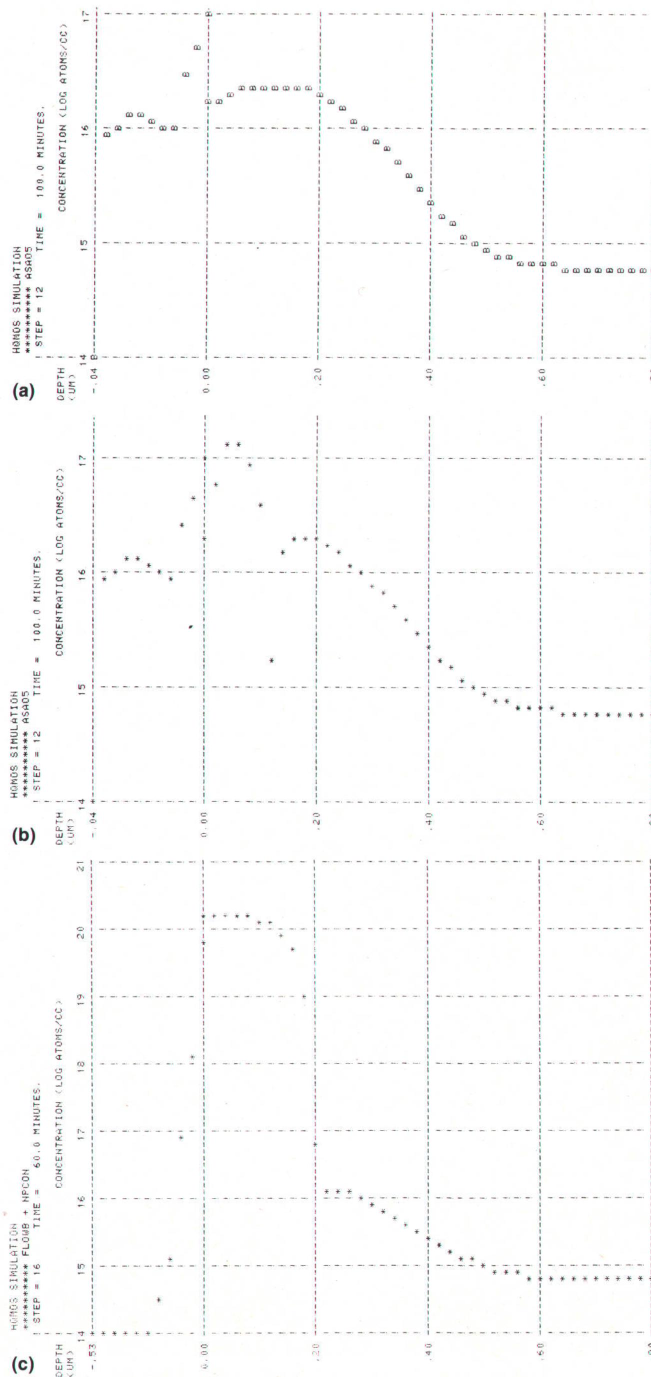

Fig. 2. *HQMOS impurity profiles from SUPREM simulations. (a) Active region of an enhancement device. (b) Active region of depletion device. (c) Source-drain n^+p junction.*

Polysilicon gates (2 μm wide) and interconnects are then patterned by another photolithographic process.

A nonundercutting dry etching process is used to etch the polysilicon layer. Fig. 1f shows the cross section after polysilicon etching. After the photoresist is removed, the entire structure is implanted with an arsenic dose of $7\times10^{15}/cm^2$ at 90 keV to form the source and drain n^+ regions as shown in Fig. 1g. This is followed by an annealing cycle at 900°C to activate the arsenic and at the same time grow a thin layer of oxide on top of the n^+ regions and polysilicon surfaces. About 500 nm of phosphorus-doped (7.5%) low-temperature oxide is then deposited on the surface. This layer of oxide acts as an insulating layer between the polysilicon and metal layers. A 900°C steam cycle is used to soften the phosphorus-doped oxide so that it will flow a little and thus smooth the steps over the polysilicon edges.

The next step is contact masking and oxide etching. A wet-dry-wet etching process was developed to create proper oxide slopes at the edge of the contact windows while maintaining proper control of the contact areas. Fig. 1h shows the cross section of the structure after contact etching. Wafers are then subjected to a short phosphorus predeposition cycle at 900°C. The purpose of this step is to form an n^+p junction where contact window openings at the edge of active regions overlap the field substrate. This avoids any shorts at the overlapped regions and allows contacts to be placed very close to or even overlap the field oxide. Before a 1-μm-thick layer of 2% silicon-doped aluminum is deposited, a brief deglazing step removes any oxide grown in the contact window. Metal lines are defined by a photolithographic process and etched in CCl_4/He plasma. A CF_4/O_2 plasma is used to etch off the silicon residue. The wafers are alloyed in a pure H_2 ambient for 30 minutes to ensure good n^+-to-metal contacts and reduce the surface states or any damage caused by the sputtering or dry etching process. The completed structure is shown in Fig. 1i. A passivation layer is not shown, but is included for scratch protection.

Table I summarizes some of the key process parameters. Only nominal values are listed here. The amount of side encroachment, 2ΔW, is obtained from electrical measurements of transistors with different channel widths W. The value of channel length reduction, 2ΔL, comes directly from the junction depths. Fig. 2a and Fig. 2b show simulated impurity profiles for the active region of the enhancement and depletion transistors, respectively. The boron concentration profile, which determines the enhancement threshold voltage as well as the source-to-drain punchthrough voltage, peaks at $2\times10^{16}/cm^3$ within a depth of 0 to 0.2 μm beneath the Si-SiO_2 interface (shown as 0.00 in the horizontal scale) and tapers off to the substrate doping level at a depth of 0.5 μm. A similar plot for a depletion transistor is shown in Fig. 2b. Here the arsenic profile is superimposed onto the boron profile. The arsenic concentration profile peaks at a depth of approximately 0.05 μm and tapers off at 0.1 μm. The source and drain n^+p junction profile is shown in Fig. 2c. The junction depth predicted by a SUPREM* simulation is only 0.2 μm. However, spreading

*A process modeling program developed at Stanford University under the sponsorship of both HP and the Advanced Research Projects Agency.

Table I
Nominal HQMOS Process Parameters

Parameter	Value
Polysilicon line/space width:	2 μm/1.5 μm
Metal line/space width:	3 μm/2 μm
Gate oxide thickness:	40 nm
Diffusion sheet resistivity:	40 Ω/□
Polysilicon sheet resistivity:	35 Ω/□
Metal (2%Si-Al) sheet resistivity:	0.03 Ω/□
Metal current density:	1×10^5 A/cm²
Junction depth (x_j):	0.3 μm
2ΔW:	1.8 μm
2ΔL ($2x_j$):	0.6 μm

resistance measurements show that a small amount of arsenic doping extends to a depth of about 0.3 μm.

Key Process Development Areas

The standard MOS device in 1976 had an effective channel length of 6 μm with 120-nm-thick gate oxide. This was reduced to 3.5 μm and 70 nm of oxide in 1977, and to 2 μm and 40 nm in 1978 (Intel's HMOSII™ process). Shorter channel lengths and thinner gate oxides are two key factors in the improvement of the process technology. Developments making them possible include:

- Fine-line lithography. The smallest line-to-line pitch used in HQMOS is 3.5 μm, with lines 2 μm wide and spaced 1.5 μm apart on the polysilicon gate level. This exceeds the capability of typical 1:1 projection mask aligners. A direct-step-on-wafer (DSW) system using 10:1 optical projection was chosen here. The 10× reticles are generated by a direct electron beam writing process to provide better mask geometry control. A positive photoresist process is required for better resolution and etch masking. In the routine operation, a level-to-level registration accuracy of 0.35 μm is adequate for the process.

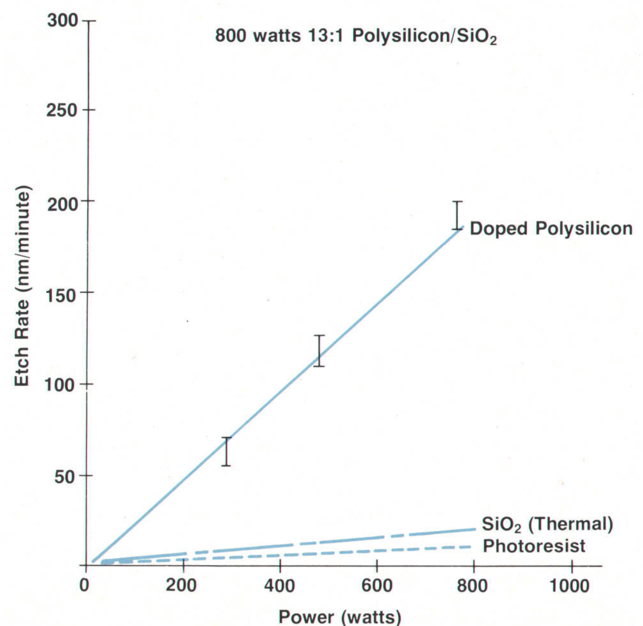

Fig. 3. *Plasma etch rates for doped polysilicon, thermal oxide, and photoresist versus RF power level.*

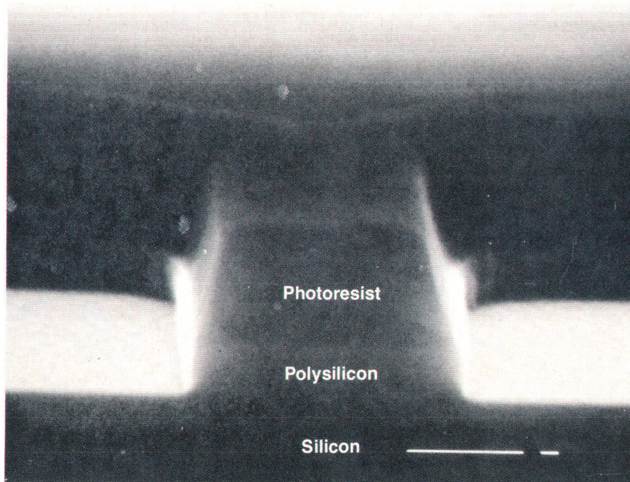

Fig. 4. *Microphotograph of a typical polysilicon etch result before photoresist is removed.*

This is the manufacturer's specification and can be improved by machine optimization and operator training. Experimental results indicate that linewidth control of 1.9±0.2 μm can be achieved.

- Dry etching of polysilicon. A nonundercutting plasma etching process was developed to etch 2-μm-wide polysilicon lines. CCl_4 vapor is introduced into an evacuated planar reactor and mixed with helium gas to maintain a stable etch gas pressure. The typical etch rate is 120 nm/minute on phosphorus-doped polysilicon using 500 watts of RF power at a gas pressure of 250 millitorr. Under a typical etching condition, no significant undercut is observed even with 100% overetch. Fig. 3 shows the etch rates of doped polysilicon, oxide, and photoresist. An etch ratio of better than 10:1 was observed between polysilicon and thermal oxide or photoresist. This differential etch ratio is more than adequate for 40 nm of oxide. Fig. 4 shows a typical etch result before the photoresist was removed. Another etch process which uses C_2F_6 gas in lieu of helium was developed by HP's Cupertino Integrated Circuit Operation. Similar results were obtained with smaller differential etch ratios. Based on electrical test data, an overall linewidth reduction of 0.1±0.2 μm was observed; this includes both photolithographic and etching components.
- Dry etching of contact oxide. There are three factors to be considered in contact oxide etching, namely, size control, edge slope, and selectivity. Since no single etch process has been found that provides an adequate solution to all of these factors, a wet-dry-wet etching process was developed to overcome the difficulties. The first wet etching step is done in a 20:1 NH_4F:HF buffered etch solution, and the dry etching step is done in C_2F_6/He plasma. The buffered etch solution etches phosphorus-doped oxide at 110 nm/minute and thermal oxide at 28 nm/minute. This was the lowest etch ratio found. This low etch ratio is important in the final wet etching step because the oxide to be etched is thermally grown on the surface of an n^+ region or polysilicon. The first wet etching step clears about one third of the total oxide thickness with some undercutting. The dry etching removes all of the remaining oxide except the last 50 nm, which is removed by wet etching. This last wet etching step overcomes the poor selectivity of the dry etch step, and also widens the edges of the contact area slightly to achieve the desired oxide slope. A slope of 50 to 60 degrees is obtained routinely by this method.
- Dry etching of aluminum. The etch gas is a mixture of CCl_4/He similar to that used for polysilicon etching. The

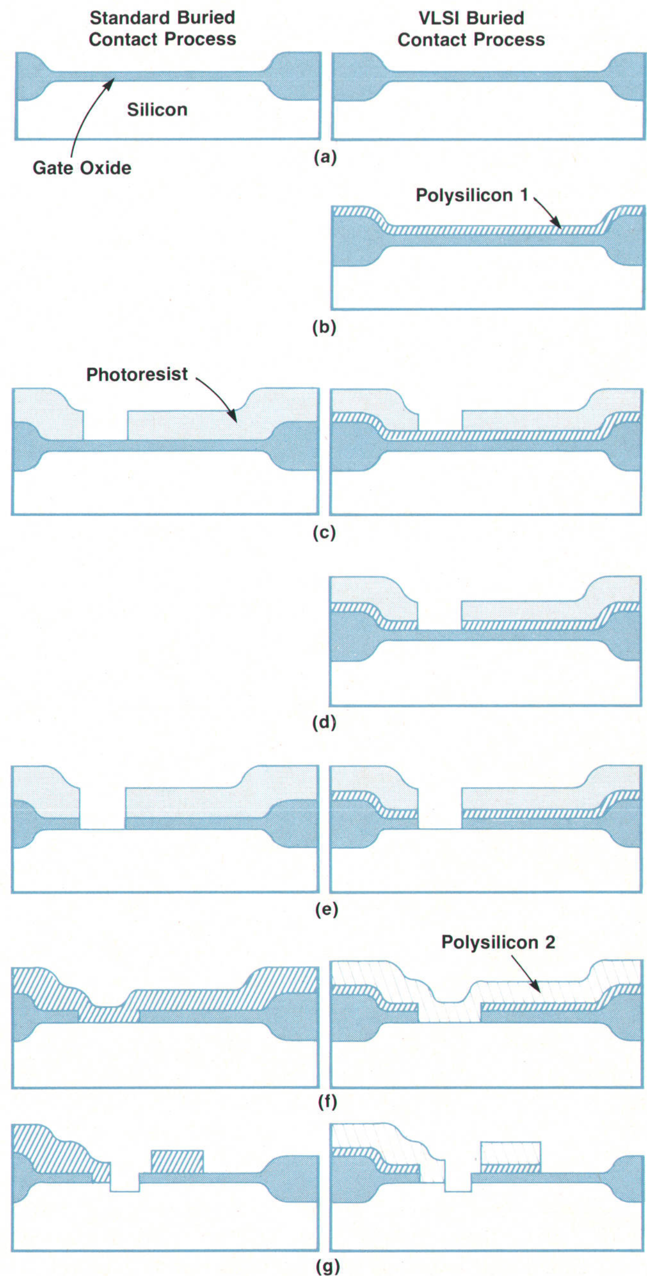

Fig. 5. *Comparison of the new buried contact process with a conventional process. (a) Gate oxide formation. (b) First polysilicon deposition. (c) Buried contact masking. (d) First polysilicon etching. (e) Contact oxide etching. (f) Resist stripping, residue oxide etching, second polysilicon deposition. (g) Polysilicon gate patterning and etching.*

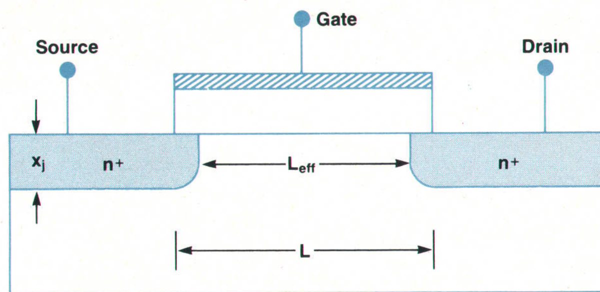

Fig. 6. *Cross section of an MOS transistor.*

typical etch rate is approximately 150 nm/minute at RF power levels from 300 to 800 watts, with better anisotropic results at higher power levels. A two-step etching method, first at 800 watts and then at 300 watts, is needed to avoid any residual aluminum rings around the steps. Etching at 800 watts not only provides an anisotropic result, but also removes any aluminum oxide on the surface. The 300-watt etch usually starts when the metal layer is etched through and provides some isotropic etching to remove residue. With optical endpoint detection, the typical undercut for 1-μm-thick aluminum is approximately 0.2 μm per edge.

- Gate oxide. The 40-nm-thick gate oxide is grown in 900°C steam followed by one hour of gettering in a dry oxygen ambient mixed with 0.63% 111-trichloroethane (TCA). Typical thickness variation from run to run is ±10% with better uniformity from wafer to wafer in a single run. Uniformity across a wafer is better than ±5%. This is important because the threshold voltage of a device is proportional to the oxide thickness. Typical fixed oxide surface charge is in the 4-to-6×10^{10}/cm^2 range. Breakdown voltage of the oxide is approximately 35 volts, which corresponds to a dielectric strength of 8.7×10^6 volts/cm. Results of bias temperature stress tests, which were done by applying an electric field of -5×10^5 volts/cm or 1×10^6 volts/cm at 300°C for five minutes and then cooling to room temperature with the electric field still applied, indicate that the oxide is relatively free from mobile ion contamination. The defect density of the gate oxide ranges from 5 to 40/cm^2. These numbers were generated from the yield data of 500-μm-by-500-μm square polysilicon gate MOS capacitors that withstand an electric field greater than 5×10^6 volts/cm.
- Buried contact process for thin gate oxides. Conventional methods for fabricating this type of contact face a severe gate oxide degradation problem when the oxide is thinner than 50 nm or so. This is because, during a short oxide etching step to remove about 3 to 5 nm of native oxide from the contact region, the oxide in the active gate is also etched. This etch reduces the strength of the oxide and increases its defect density.

The new process uses a thin layer of polysilicon to protect the gate oxide during the short etch operation. Fig. 5 shows the steps of the new process compared to the conventional approach. Only two extra steps are needed for the new process, namely, deposition of the first polysilicon layer and the etching of the layer. No extra masking is involved. Test results have shown that about 50 to 70 nm of polysilicon is adequate for the purpose. Too thick a polysilicon layer results in removing too much of the silicon substrate during the etching step to pattern the gate electrodes.

- Shallow junction formation. Fig. 6 shows the cross section of a transistor. The effective channel length L_{eff} is related to polysilicon gate length L and the junction depth x_j by

$$L_{eff}=L-2x_j, \tag{1}$$

assuming the lateral outdiffusion of an n^+ layer is the same as the vertical diffusion. In a positive photoresist process, L is typically 1.9±0.2 μm for a 2-μm mask geometry. With nonundercutting dry etching, this L value can be reproduced with no more than 0.1 μm shrinkage. For $x_j = 0.3$ μm, L_{eff} should be 1.1 to 1.5 μm for a 2-μm mask size. In addition to doping the contact region with phosphorus after contact etching (to ensure at least a 0.3-to-0.4-μm-thick n^+ layer at the contact), the aluminum metallization is also doped 2% with silicon to avoid problems where the aluminum dissolves some of the underlying silicon material and, in some cases, can reach a junction and short it out.
- Low-temperature phosphorus-doped oxide flow. To ensure proper metal step coverage at any step, the phosphorus-doped oxide layer must be softened at an elevated temperature so that it will flow to provide a smoother surface. The higher the temperature, the smoother the surface is going to be. However, if the temperature is too high, the diffused junctions will be affected. A 900°C steam process was developed for this purpose so that the overall heat treatment can be kept to a minimum. Fig. 7 shows the surface topography of the finished devices with 7.5% phosphorus-doped oxide. Excellent metal step coverage is achieved here.

Device Characteristics

When an MOS device is operating in the electron velocity saturation mode, the maximum source-to-drain current

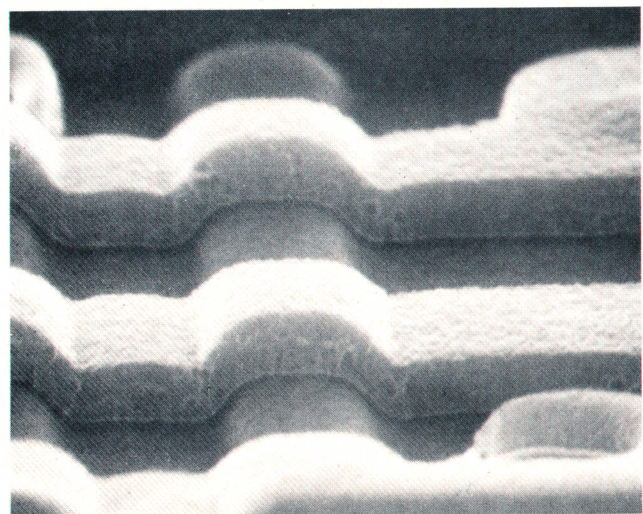

Fig. 7. *Microphotograph of finished device surface topography. The phosphorus doping level is 7.5%.*

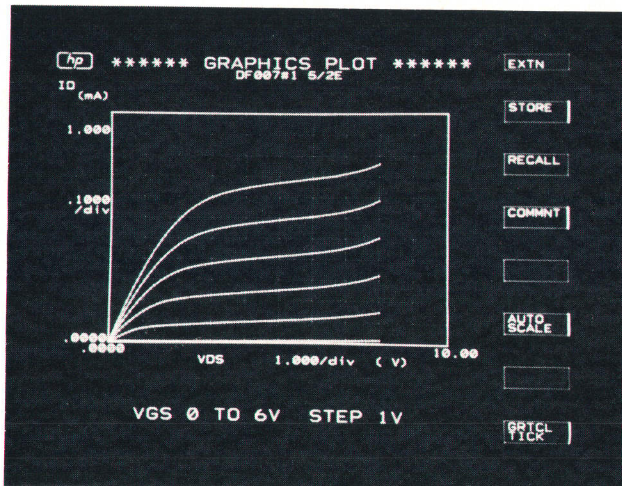

Fig. 8. *I-V characteristic of an HQMOS device (W/L=5/2). (Evaluated by the 4145A Semiconductor Parameter Analyzer described in this issue.)*

I_{max} is given by[3]

$$I_{max} = K\ v_{sat} W' C_o\ (V_{GS} - V_T) \qquad (2)$$

where v_{sat} is the saturation velocity of electrons, W' is the effective channel width, C_o is the gate oxide capacitance, V_{GS} is the voltage between source and gate, V_T is the threshold voltage of the transistor, and K is a figure of merit for the given device design. The exact value of K is determined by the vertical impurity profile and the normalized capacitance. The value for K ranges from 0.0 to 1.0.

Equation (2) indicates that the source-to-drain current is linearly proportional to the gate voltage, which is different from that for a long-channel device. In the latter case, the current is proportional to the square of gate voltage. The typical I-V characteristic of an HQMOS device is shown in Fig. 8. For L = 2 μm, the device is operating in the velocity saturation mode. The K value for the device can be obtained from equation (2) by taking the difference between two currents and dividing by the corresponding difference in two voltages. Typically, $v_{sat} = 9 \times 10^6$ cm/s, and K is approximately 0.5.

The threshold voltage of a device is very sensitive to channel length variations, especially when the length is less than 5 μm (Fig. 9a). The threshold voltage is also sensitive to the channel width W when W is less than 5 μm (Fig. 9b). Encroachments into the channel width come from the lateral diffusion of implanted boron during field oxidation. Substrate bias also greatly affects the threshold voltage. This effect is illustrated in Fig. 9c, where V_T is plotted versus the square root of $-V_{sub}+2|\phi_F|$. ϕ_F is the Fermi level of the substrate and V_{sub} is the substrate bias voltage. There are two slopes in the plot. One corresponds to the higher doping level near the silicon-to-silicon-dioxide interface and the other corresponds to the substrate doping. The shoulder region corresponds to the junction between the implanted boron and the substrate. Table II lists some electrical parameters of the HQMOS devices. Subthreshold slopes are relatively independent of device gate length and are 80 mV/decade and 90 mV/decade for the enhancement and depletion transistors, respectively. Table III lists a set of SPICE parameters generated by matching the device models with experimental results. Because of nonuniform boron doping near the surface, the V_{T0} value is different from the actual threshold voltage measured at zero substrate bias voltage.

A 21-stage ring oscillator, with pull-up depletion load (W/L=3/2) and pull-down enhancement (W/L=5/2) devices, was used to estimate the gate delay and power consumption of an HQMOS inverter. With V_{DD} = 3 volts and $V_{sub}=-2$ volts, the typical gate delay per stage is approximately 450 picoseconds, and the delay-power product is approximately 80 femtojoules.

The first IC chip designed using the HQMOS process is a digital filter chip. This chip contains approximately 42,500

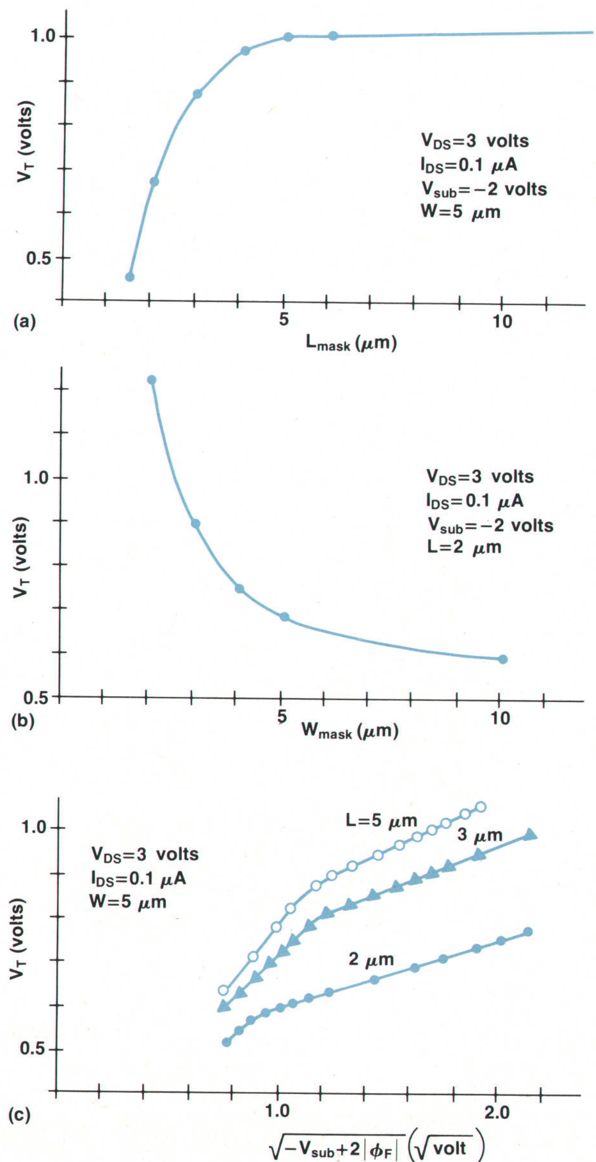

Fig. 9. *Changes in threshold voltage caused by (a) channel length variation, (b) channel width variation, and (c) substrate bias level.*

Table II
Nominal HQMOS Electrical Parameters

V_{DD}:	3V
V_{sub}:	−2V
V_T (enhancement, W/L=5/2):	0.6V @ $V_{sub}=-2V$
V_{Depl1} (W/L=5/2):	−1.5V @ $V_{sub}=-2V$
V_{Depl2} (optional W/L=3/5):	−0.5V @ $V_{sub}=-2V$
Subthreshold slope (L=2 μm):	
Enhancement:	80 mV/decade
Depletion:	90 mV/decade

Table III
Extracted SPICE Parameters

Enhancement device (W/L=5/2):

$\mu_o = 550\ cm^2/V\text{-}s$	$t_{ox} = 36\ nm$
$V_{T0} = 0.69V$	$R_s = 0$
$N_{sub} = 1.1\times10^{15}/cm^3$	$R_d = 0$
$V_{norm} = 22.5V$	
$D_{esat} = 1.00\times10^9 V/cm^2$	$L_d(\Delta L) = 0.38\ \mu m$
$E_{crit} = 1.0\times10^5 V/cm$	$W_d(\Delta W) = 0.95\ \mu m$
$E_{tra} = 5\times10^4 V/cm$	

transistors and operates at a 20-MHz clock rate. A very fast digital-to-analog converter and 4-bit shift registers and latches operated at 180 MHz have been demonstrated by various groups within HP Laboratories.

Acknowledgments

The development effort was carried out by Hewlett-Packard's Integrated Circuit Laboratory (ICL) in conjunction with the then Instrument Research Laboratory (IRL, now Measurement and Communication Laboratory) and the Santa Clara Division. Process development work and device modeling and characterizations were done in ICL with the help of IRL in device and SPICE modeling. Circuit designs were done in Santa Clara Division, also with help from IRL. All wafer processing was done in HP's Integrated Circuit Processing Laboratory (ICPL). The initial phase of the development work was carried out under the guidance of Juliana Manoliu. Kuang Chiu's participation in the early development work is also acknowledged. Many thanks to Fred Schwettmann, Dirk Bartelink, Pat Castro, John Moll, and Bob Grimm for their support and encouragement during the course of this work.

References

1. R. Dennard, et al, "Design of Ion Implanted MOSFETs with Very Small Physical Dimensions," IEEE Journal of Solid-State Circuits, Vol. SC-9, no. 5, October 1974.
2. R. Szeto, et al, "A Buried Contact Process for VLSI," to be presented at the Fall Meeting of the Electrochemical Society, paper 175, Detroit, Michigan, October 1982.
3. J. Moll, "Outer Limits of VLSI," presented at Semiconductor Interface Specialist Conference, New Orleans, Louisiana, November 29, 1979.

Roger To-Hoi Szeto

Roger Szeto attended the University of California at Berkeley, earning the BS (1977) and MS (1980) degrees in chemical engineering. He joined HP in 1980 and his work in NMOS process development has resulted in two papers. Roger is a native of Hong Kong and enjoys fishing and bowling. He lives in San Francisco, California.

Devereaux C. Chen

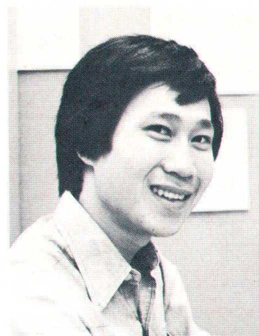

Dev Chen joined HP in 1981 after earning the MSc degree in electrical engineering at Yale University. He also holds the BS degree in physics/electronics awarded by the University of Manchester, United Kingdom, in 1979. His work at HP is concerned with NMOS process development. Dev was born in Kingston, Jamaica, and now lives in Mountain View, California. He enjoys playing soccer, riding bicycles, working with computers, and playing guitar.

Anders T. Dejenfelt

Anders Dejenfelt was born in Mörard, Malmö, Sweden and attended Lund Institute of Technology, Lund, Sweden, earning an MS degree in applied physics in 1977. After two years doing development work in Sweden on high-power thyristors, he joined HP in 1979 as a member of the technical staff at HP Laboratories. Until he left HP recently to work on custom IC designs, his work involved MOS device characterization and modeling. Anders is a member of the IEEE and lives in Los Altos, California. He is interested in fast cars, board sailing, playing guitar, and skiing.

Horng-Sen Fu

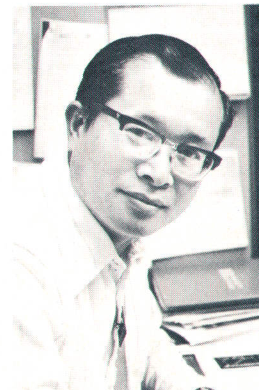

Horng-Sen Fu received the PhD degree in electrical engineering from the University of Illinois at Urbana-Champaign in 1971. He performed research on MOS devices and physics there until 1973. He joined HP in 1978 after five years of doing R&D work on CCD memories for a major semiconductor manufacturer. Horng-Sen is now a project manager in HP Laboratories responsible for developing high-performance NMOS devices and circuits. His work has resulted in eight patents related to MOS technology and over 20 articles and conference papers about semiconductor device physics and processing. Horng-Sen was born in Taiwan and is a member of the IEEE and the Electrochemical Society. He is married, has three children, and lives in Sunnyvale, California.

MOS Device and Process Design Using Computer Simulations

By using carefully developed computer models, IC device performance can be accurately simulated and the effects of process changes predicted, saving time and expense in new product design and development.

by Soo-Young Oh

METAL-OXIDE-SEMICONDUCTOR field-effect transistors (MOSFETs), first proposed 50 years ago, are based on the principle of modulating longitudinal electrical conductance by varying a transverse electric field. Since its conception, MOSFET technology has improved steadily and become the primary technology for large-scale circuit integration on a monolithic chip, primarily because of the simple device structure. VLSI (very large-scale integration) development for greater functional complexity and circuit performance on a single chip is strongly motivated by the reduced cost per device and has been achieved in part by larger chip areas, but predominantly by smaller device dimensions and the clever design of devices and circuits.

As a consequence of reduced device dimensions, a small two-dimensional (or even three-dimensional) MOSFET structure has evolved. Scaling down dimensions introduces problems in both fabrication and operation that are not significant in larger long-channel devices. The two-dimensional aspects of the impurity profiles and oxidation processes become important in determining the effective channel length and width. More processing steps are required, such as channel implantation and local oxidation, which make more stringent control of the process necessary. Secondary effects such as oxidation-enhanced diffusion significantly affect the impurity profile. As a result, better understanding and accurate control of these phenomena are crucial to achieving the desired performance from scaled-down devices.

Device operation reveals the existence of two-dimensional field coupling involving both the short-channel and narrow-width effects. This may not be a problem if the ideal scaling-down theory[1] is followed because, in concept, all dimensions and impurity profiles are scaled so as to maintain the same electric field pattern as for a long-channel device. However, this is not typically followed because of practical limitations such as retaining a standard 5V operating voltage, and requiring thicker oxides to prevent gate breakdown. Device characteristics are highly dependent, therefore, on the two-dimensional structure; classical analysis based on the one-dimensional model is not valid.

Conventional process and device designs for integrated circuit technologies have been based on the use of a trial-and-error approach and simple analytical modeling to achieve the desired electrical characteristics and circuit performance. The left half of Fig. 1 outlines a systematic

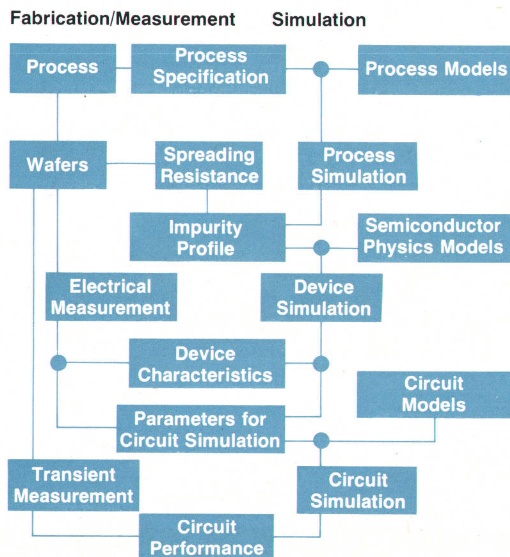

Fig. 1. *Block diagram of MOS process, device, and circuit design paths. The left-hand path shows the traditional trial-and-error approach and the right-hand path illustrates the simulation approach.*

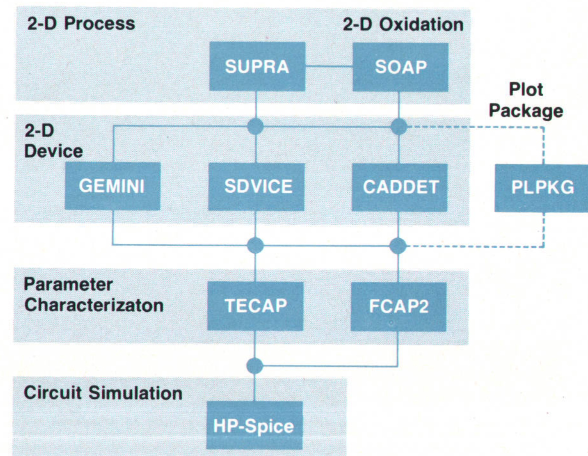

Fig. 2. *Block diagram of two-dimensional simulation system.*

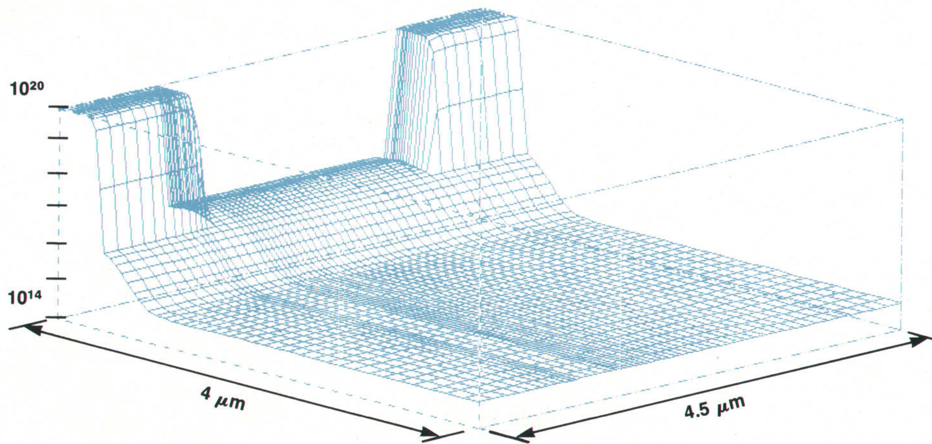

Fig. 3. *Simulated two-dimensional impurity distribution for a standard NMOS device with a 2.5-μm channel length.*

procedure for process, device, and circuit design using both trial-and-error and experimental measurement. This approach is not adequate, however, for small-geometry MOSFETs where process complexity (especially patterning and tolerance requirements) and two-dimensional field coupling prevent the use of a simple one-dimensional analysis for obtaining accurate quantitative information. In addition, the purely experimental approach yields little physical insight into the factors governing device operation. However, it is well suited for later design cycles where final parameter adjustments can be accommodated. A complementary analysis and design path (right half of Fig. 1) using process, device, and circuit simulations has been proposed and is now widely accepted. Compared to laboratory experimentation, the design path via simulation is less costly and faster. More important, it produces detailed information about device operation in a well-controlled environment.

Two-Dimensional Simulation System

Many two-dimensional device simulation programs have been developed and several reported recently. These programs, however, are research tools rather than design tools. More stress has been put on the development of fast algorithms and the implementation of the physical mechanism than on the user interface. Furthermore, each program was developed independently without an interface to other programs. Thus, transferring massive amounts of two-dimensional numerical data from one program to another is very difficult. Analyzing and interpreting the data is also difficult. To overcome these problems and provide a convenient design path using simulation, a complete two-dimensional simulation system has been developed and implemented at HP with an emphasis on the user interface. The following schemes have been adopted to make this system a more practical and user-oriented design tool.

- All programs are on an HP 1000 Computer for fast turnaround
- Friendly, interactive input/output
- Data transfer between programs using standard-format disc files that are transparent to the user
- Graphic plotting capability accessible to all two-dimensional programs to process and analyze the massive amounts of data generated by these programs
- Hierarchical simulations are used wherever possible because full two-dimensional simulations are time consuming.

A block diagram of this system is shown in Fig. 2. The process simulator SUPRA (Stanford University Process Analysis program)[2] simulates processes based on the device geometry and process schedule and generates the impurity distributions. SUPRA can handle deposition, etch, ion implant, diffusion and oxidation process cycles. The oxidation model is based on empirical data. For impurity diffusions. SUPRA analytically solves the diffusion equation using a constant diffusivity for low impurity concen-

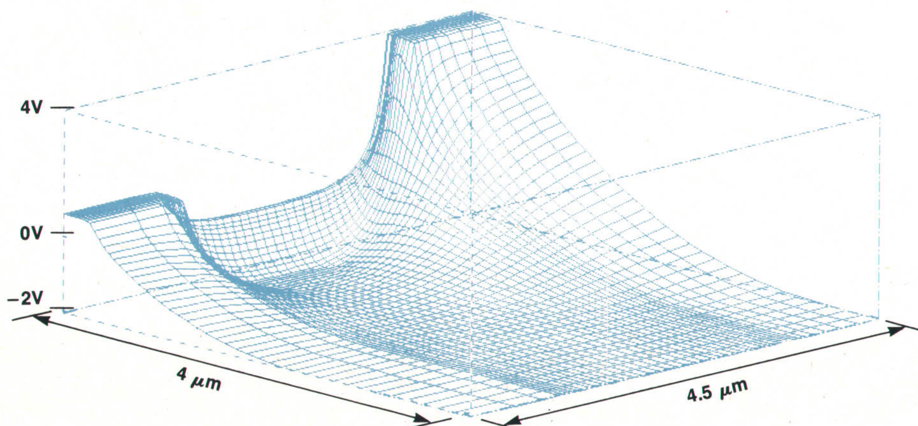

Fig. 4. *Simulated two-dimensional potential distribution for a standard NMOS device. Channel length L=2.5 μm, V_{GS}=−0.2V, V_{DS}=3V, and V_{BS}=−2V.*

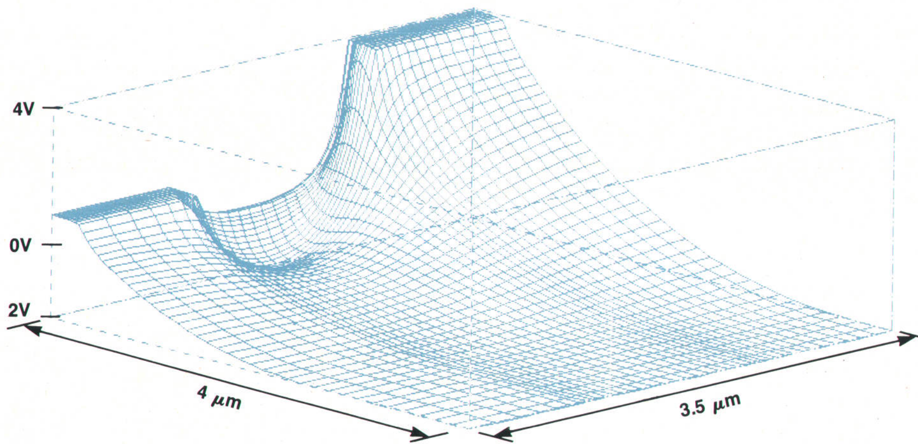

Fig. 5. Potential distribution for scaled-down NMOS device (HQMOS, channel length reduced to 1.5 μm and using same voltages as for Fig. 4).

trations. For higher concentrations, it solves the diffusion equation using a concentration-dependent diffusivity in a numerical finite-difference method. For a more accurate two-dimensional oxidation simulation, SOAP should be used. SOAP is a program that simulates the diffusion of the oxygen in the oxide and the propagation of the extra oxide volume generated during the oxidation in a rigorous manner. Two-dimensional oxidation is a difficult problem to simulate because of nonplanar geometries and moving boundaries. SOAP uses the boundary-value (BV) method. In this method, the nodes are allocated only along the boundary. Thus, it is very suitable for nonplanar geometry and moving-boundary problems.

Electrical device characteristics are predicted by two-dimensional device simulators based on the impurity distributions predicted by SUPRA. In these device simulations, the Poisson and current continuity equations should be solved with the appropriate boundary conditions to be valid over the whole operating region of MOS transistors. Such an algorithm is used by the full two-dimensional simulator CADDET.[3] The full simulator, however, is slow and a simplified analysis should be used whenever possible (hierarchial simulations). For the subthreshold region where the current is small, the two-dimensional Poisson-equation solver GEMINI[4] is fast and accurate enough for most applications. For a large number of simulations, such as I-V characteristic generation, SDVICE is accurate enough. SDVICE numerically solves the one-dimensional current-continuity equations along the channel with appropriate two-dimensional field coupling to the boundary conditions using the boundary-value method as mentioned above. In the BV method, because the nodes are allocated only along the boundaries and the channel, a much smaller number of nodes are required than for the finite-difference or finite-element methods. Furthermore, a fast two-dimensional Poisson-equation solver has been incorporated to enhance the accuracy for nonuniform substrate doping. The calculation speed of this method is an order of magnitude faster than that of the full two-dimensional simulator.

Based on the device characteristics calculated by these simulations, the electrical parameters can be extracted by TECAP[5] for use in circuit simulations. TECAP measures the device characteristics of MOS and bipolar transistors and extracts their parameters. Here, the data is taken from the simulation and only the parameter extraction part of TECAP is used. In VLSI circuits, accurate determination of interconnect and other capacitance values becomes crucial in the circuit simulation. The value of various capacitance components in MOS circuits can be simulated and determined by FCAP2, a two-dimensional, arbitrary-geometry, linear-Poisson-equation solver. The circuit performance can be simulated by HP-SPICE,[6] based on electrical parameters and capacitances that were obtained from the process schedule and device layout using this simulation system.

Application Examples

An example of an application of this simulation system is the scaling down of a standard n-channel MOS process (see

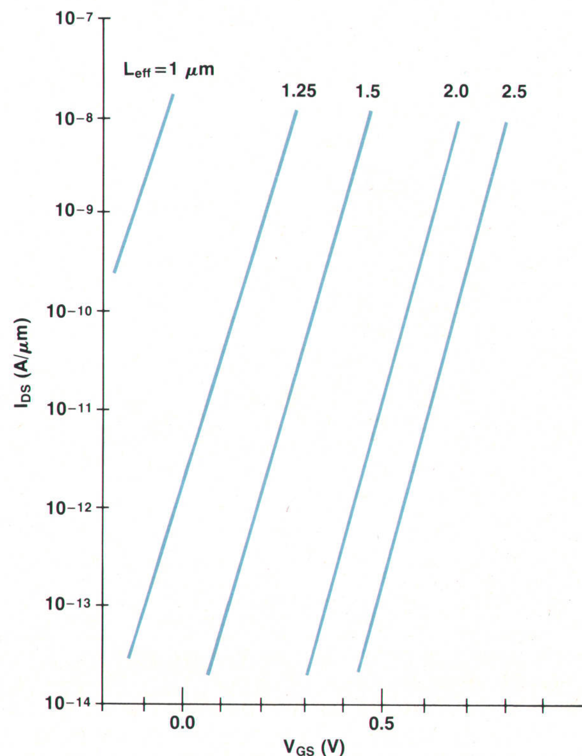

Fig. 6. Effects of variations in effective channel length on subthreshold MOS device characteristics.

article on page 21) from 2.5 μm to 1.5 μm. The impurity distribution simulated by SUPRA for the standard NMOS process is shown in Fig. 3.

To simulate the scaled-down process, the mask channel length is first reduced from 2.5 μm to 1.5 μm while all the process steps remain the same. Fig. 4 and Fig. 5 show the simulated potential distribution of 2.5-μm and 1.5-μm channel length devices with $V_{GS}=-0.2V$, $V_{DS}=3V$ and $V_{BS}=-2V$. Because stronger two-dimensional field coupling is evident in Fig. 5 where the mask channel length is shorter, the threshold voltage V_T is lower for the shorter device. In Fig. 6, the I_{DS}-versus-V_{GS} characteristic is simulated by GEMINI for various channel lengths to show the effect of channel length on V_T. The V_T of a 1.5-μm device is shifted by 0.34V from that of a 2.5-μm device.

Next, the gate oxide is scaled down from 40 nm to 30 nm and the resulting changes in the subthreshold characteristics are shown in Fig. 7. Because of the lower body effect caused by the higher gate capacitance, V_T is lowered farther by 0.18V. To maintain the same threshold voltage in the scaled-down device, the dose of the channel implantation must be changed. The subthreshold characteristics for several different doses and the corresponding impurity profiles were obtained by using SUPRA and GEMINI. The optimum dose was found to be $1.2\times10^{12}/cm^2$. The subthreshold characteristics of the scaled-down device with this dose are shown by curve (d) in Fig. 7.

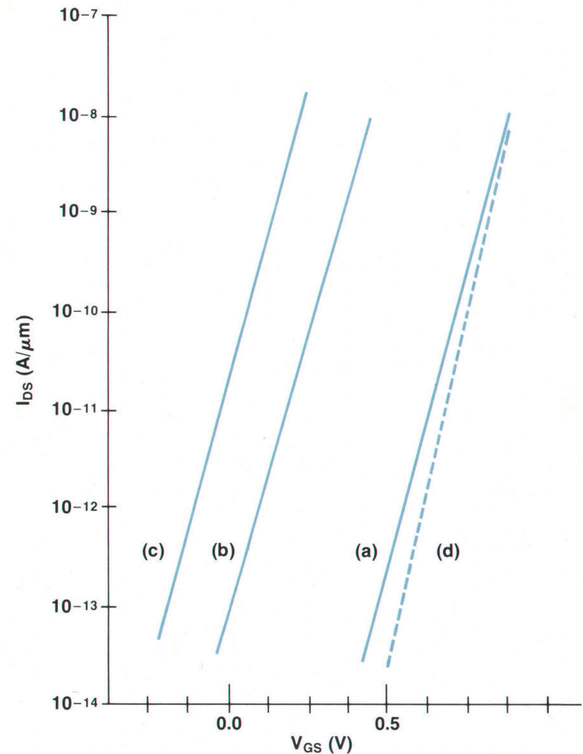

Fig. 7. *Subthreshold characteristics as function of channel length L, gate oxide thickness t_{ox}, and channel implant dose.*
(a) L=2.5 μm, t_{ox}=40 nm, dose=$7\times10^{11}/cm^2$
(b) L=1.5 μm, t_{ox}=40 nm, dose=$7\times10^{11}/cm^2$
(c) L=1.5 μm, t_{ox}=30 nm, dose=$7\times10^{11}/cm^2$
(d) L=1.5 μm, t_{ox}=30 nm, dose=$1.2\times10^{12}/cm^2$

Another example involves the two-dimensional semirecessed field oxidation used for device isolation in an NMOS process. As shown in Fig. 8 (simulation), the field oxide layer grows laterally (bird's beak) under the silicon-nitride mask and reduces the effective channel width significantly. The penetration distance ΔW is a function of oxidation temperature, oxidation time, and the thickness of the nitride mask. SOAP calculates the diffusion of the oxygen from the oxide surface to the silicon-oxide interface and the growth of the extra oxide volume generated during the oxidation, including the stress of the nitride layer. It accurately simulates the effects of the oxidation temperature, oxidation time, and the nitride thickness on the lateral shape and penetration of the field oxide. In the example shown in Fig. 8, a 0.95-μm-thick field oxide is grown using a two-hour wet oxidation cycle at a temperature of 1000°C. The thickness of the nitride layer is 50 nm. The lateral penetration ΔW is 0.8 μm. The simulated result agrees well with actual results observed by a scanning electron microscope.

A third example is the calculation of the parasitic capacitance of the interconnect line for the HQMOS process using FCAP2. When the width of the interconnect line decreases, the capacitance of the line does not decrease linearly because of fringing electric field effects at the edges of the line. Fig. 9 shows the equipotential lines for the 1.8-μm-wide polysilicon line as simulated by FCAP2. The thickness of

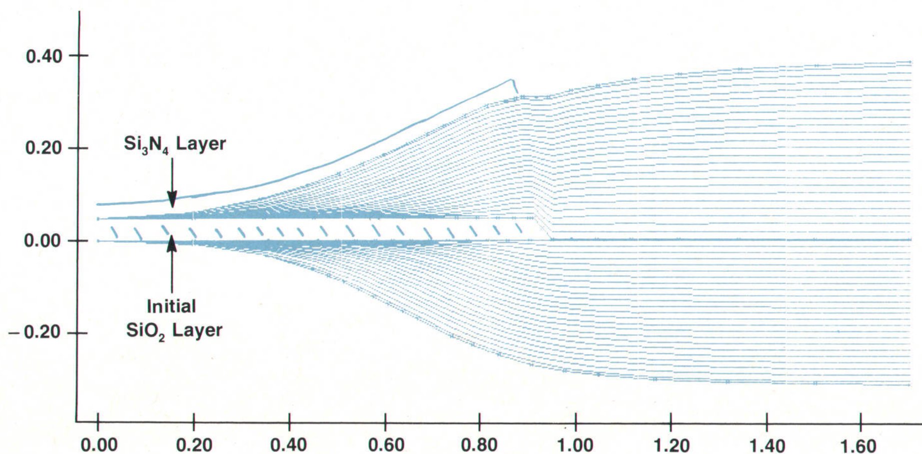

Fig. 8. *Two-dimensional simulation of semirecessed field oxidation process used for NMOS device isolation. Temperature =1000°C, oxidation time =120 minutes.*

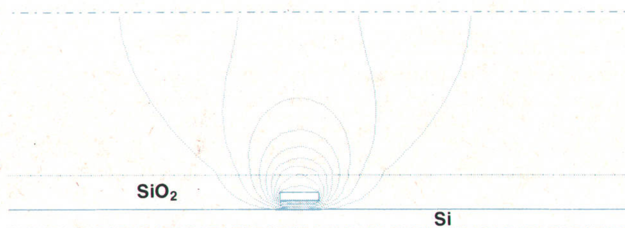

Fig. 9. *Parasitic capacitance calculation by FCAP2 for polysilicon line used in HQMOS circuits. Field oxide thickness=0.4 μm, polysilicon thickness =0.4 μm, and linewidth =1.8 μm.*

the field oxide between the polysilicon and the substrate is 0.4 μm. The polysilicon line is also 0.4 μm thick. The calculated capacitance of this line is 0.117×10^{-3} pF/μm, using the one-dimensional parallel-plate approximation. The actual measured capacitance, which includes the fringing-field effects, is 0.196×10^{-3} pF/μm. The fringing field increases the capacitance by 67.5%.

Acknowledgments

GEMINI, SUPRA and TECAP are programs that have been developed at Stanford University under the direction of Bob Dutton and sponsored by both HP and the Advanced Research Projects Agency. CADDET is a program developed by Hitachi Company in Japan.

References

1. R.H. Dennard, et al, "Design of Ion-Implanted MOSFETs with Very Small Physical Dimensions," IEEE Journal of Solid-State Circuits, Vol. SC-9, October 1974, pp. 256-268.
2. D. Chin, M. Kump, and R.W. Dutton, "SUPRA: Stanford University Process Analysis Program," Stanford Electronics Laboratories, Stanford University, Stanford, California, October 1979.
3. T. Toyabe, et al, "A Numerical Model of Avalanche Breakdown in MOSFETs," IEEE Transactions on Electron Devices, Vol. ED-25, 1978, pp. 825-831.
4. J.A. Greenfield, S.E. Hansen, and R.W. Dutton, "Two-Dimensional Analysis for Device Modeling," Technical Report No. G201-7, Stanford Electronics Laboratories, Stanford University, Stanford, California, 1980.
5. E. Khalily, "T.E.C.A.P.: An Automated Characterization System," Technical Report No. 5017-1, Stanford Electronics Laboratories, Stanford University, Stanford, California, 1980, and "Transistor Electrical Characterization and Analysis Program," Hewlett-Packard Journal, Vol. 32, no. 6, June 1981.
6. L.K. Scheffer, R.I. Dowell, and R.M. Apte, "Design and Simulation of VLSI Circuits," Hewlett-Packard Journal, Vol. 32, no. 6, June 1981, and *HP-SPICE User's Manual*, DA320.3C, Hewlett-Packard Design Aids, October 1980.

Soo-Young Oh

Soo-Young Oh was born in Seoul, Korea, and attended Seoul National University, earning a BS degree in 1972. He continued his studies at Stanford University, earning an MS degree (1976) and a PhD degree (1980) in electrical engineering. Soo-Young joined HP in 1980 and is a project leader for device and process modeling. He has written two papers on two-dimensional device simulation and is a member of the IEEE. Soo-Young lives in Union City, California, is married, and enjoys playing tennis.

Hewlett-Packard Company, 3000 Hanover Street, Palo Alto, California 94304

Bulk Rate
U.S. Postage
Paid
Hewlett-Packard
Company

HEWLETT-PACKARD JOURNAL

OCTOBER 1982 Volume 33 • Number 10
Technical Information from the Laboratories of Hewlett-Packard Company
Hewlett-Packard Company, 3000 Hanover Street
Palo Alto, California 94304 U.S.A.
Hewlett-Packard Central Mailing Department
Van Heuven Goedhartlaan 121
1181 KK Amstelveen, The Netherlands
Yokogawa-Hewlett-Packard Ltd., Suginami-Ku Tokyo 168 Japan
Hewlett-Packard (Canada) Ltd.
6877 Goreway Drive, Mississauga, Ontario L4V 1M8 Canada

CHANGE OF ADDRESS: To change your address or delete your name from our mailing list please send us your old address label. Send changes to Hewlett-Packard Journal, 3000 Hanover Street, Palo Alto, California 94304 U.S.A. Allow 60 days.

5953-8504